

1 This manuscript has been submitted for publication in GEOMORPHOLOGY. Please note that, despite having undergone peer-  
2 review, the manuscript has yet to be formally accepted for publication. Subsequent versions of this manuscript may have slightly  
3 different content. If accepted, the final version of this manuscript will be available via the 'Peer-reviewed Publication DOI' link on the  
4 right-hand side of this webpage. Please feel free to contact any of the authors; we welcome feedback.

5

6

7

8 **Modeling the spatial dynamics of marsh ponds in New England salt marshes**

9

10 G. Mariotti<sup>1,2</sup>, A.C. Spivak<sup>3</sup>, S.Y. Luk<sup>4</sup>, G. Ceccherini<sup>5</sup>, M. Tyrrell<sup>6</sup>, M. Eagle Gonneea<sup>7</sup>

11

12 1. Louisiana State University, Department of Oceanography and Coastal Sciences, Baton Rouge (LA),

13

USA

14 2. Louisiana State University, Center for Computation and Technology, Baton Rouge (LA), USA

15

3. University of Georgia, Department of Marine Sciences, Athens (GA), USA

16 4. Woods Hole Oceanographic Institution, Department of Marine Chemistry and Geochemistry, Woods

17

Hole (MA), USA

18

5. Joint Research Centre, Bioeconomy Unit, European Commission, Ispra, Italy

19

6. Waquoit Bay National Estuarine Research Reserve, Falmouth (MA), USA

20

7. U.S. Geological Survey, Woods Hole (MA), USA

21

22

**Abstract**

23 Ponds are common features on salt marshes, yet it is unclear how they affect large-scale marsh evolution.

24 We developed a spatially explicit model that combines cellular automata for pond formation, expansion,

25 and drainage, and partial differential equations for elevation dynamics. We use the mesotidal Barnstable

26 marsh (MA, USA) as a case study, for which we measured pond expansion rate by remote sensing

27 analysis over a 41-year time span. We estimated pond formation rate by comparing observed and modeled

28 pond size distribution, and predicted pond deepening by comparing modeled and measured pond depth.

29 The Barnstable marsh is currently in the pond recovery regime, i.e., every pond revegetates and recovers

30 the necessary elevation to support plant growth after re-connecting to the channel network. This pond

31 dynamic creates an equivalent (i.e., spatially and temporally averaged over the whole marsh) 0.5-2 mm/yr  
32 elevation loss that needs to be supplemented by excess vertical accretion. We explore how the pond  
33 regime would change with decreased sediment supply and increased relative sea-level rise (RSLR) rate,  
34 focusing on the case in which the vegetated marsh keeps pace with RSLR. When the RSLR rate remains  
35 below the minimum unvegetated deposition rate, the pond dynamics is nearly unaltered and ponds always  
36 occupy ~10% of the marsh area. However, when RSLR rate exceeds this threshold, the ponds in the  
37 marsh interior – which receive the least amount of suspended sediment – do not recover after drainage.  
38 These ponds transition to mudflats and permanently occupy up to 30% of the marsh area depending on  
39 RSLR rate. For marshes with a small tidal range, such as the microtidal Sage Lot Pond marsh on the  
40 opposite side of the peninsula from Barnstable marsh, high RSLR rates could bring every portion of the  
41 marsh into the pond runaway regime, with the whole marsh eventually converting into mudflats. In this  
42 regime, the existing marsh would disappear within centuries to millennia depending on the RSLR rate.  
43 Because of the spatial and temporal components of marsh evolution, a single RSLR threshold value  
44 applied across the entire marsh landscape provides a limited description of the marsh vulnerability to  
45 RSLR.

46

47

48

49

## 50 **1. Introduction**

51 Marsh evolution models commonly assume a homogenous marsh platform, in which both elevation and  
52 plant biomass change smoothly except close to a few ecotones (Marani et al., 2013). On the contrary,  
53 many marsh platforms are highly heterogeneous because of the presence of ponds – semicircular  
54 depressions permanently inundated even at low tide. This heterogeneity is particularly relevant for the  
55 Mid-Atlantic and New England coast of the USA, where ponds are ubiquitous features (Adamowicz and  
56 Roman, 2005; Harshberger, 1909; Koop-Jakobsen and Gutbrod, 2019; Redfield, 1972; Schepers et al.,  
57 2017). Thus, considering the presence of ponds is necessary to accurately predict the landscape-level  
58 evolution and persistence of these salt marshes under climate change.

59 Ponds haven been simulated in a simplified 2D model (Kirwan et al., 2008) by lowering the elevation and  
60 preventing vegetation growth in a few random locations on the marsh platform. After this temporary  
61 disturbance, the vegetation was allowed to regrow and the bed quickly regained its original elevation by  
62 accreting faster than RSLR rate. Because of these localized and temporary bursts of vertical accretion, the  
63 model provided a simple explanation for the presence of spatial heterogeneities in marsh vertical  
64 accretion and for the widely observed mismatch between marsh vertical accretion and RSLR.  
65 Nonetheless, the model overlooked several physically-based processes that play a key role in pond  
66 dynamics: pond deepening by organic matter oxidation, pond expansion by erosion of the pond edge, and  
67 pond drainage by channel interception.

68 A simple lumped model that considered the evolution of a single pond (Mariotti, 2016) suggested that  
69 marshes are either in a regime of pond recovery where ponds form, expand, reconnect with the nearby  
70 tidal creek and recover to the surrounding marsh elevation, or in a regime of pond runaway (also called  
71 pond collapse regime) in which ponds do not revegetate and marsh area is lost even if the vegetated  
72 platform keeps pace with sea-level rise. Vertical accretion by *in situ* plant production does not contribute  
73 to pond recovery if, at the time of pond drainage, the elevation of the pond bed is below the limit for  
74 vegetation growth, which is roughly equal to mean sea level along the Atlantic and Gulf Coast of the

75 USA (McKee and Patrick, 1988). Indeed, if the bed elevation lies below the limit for vegetation growth,  
76 vertical accretion is only provided by deposition of suspended sediment. Vertical accretion by *in situ* plant  
77 production would be present only after the elevation deficit for vegetation growth is overcome.  
78 Accordingly, the model found that the marsh enters the pond runaway regime when the RSLR rate is  
79 larger than the minimum unvegetated accretion rate (Mariotti, 2016), which is equal to  $C \cdot r / (2T \cdot \rho_m)$ , where  
80  $C$  is the suspended sediment concentration,  $r$  is the tidal range,  $T$  is the tidal period, and  $\rho_m$  is the mud dry  
81 bulk density. Marshes are thus more likely to be in the pond runaway regime if the tidal range is small,  
82 but a very large sediment supply can allow for pond recovery in microtidal systems, as shown by an  
83 example in coastal Louisiana (Mariotti, 2016). A major limitation of the model, however, was that it  
84 neglected the interactions between multiple ponds, which likely represent important spatial dynamics over  
85 long time scales. As a consequence, the model was not able to predict spatially averaged metrics, such as  
86 the amount of pond area on the marsh platform in the pond recovery regime or the rate of pond area  
87 increase in the pond runaway regime.

88 When considering the dynamics of ponds, it is also important to simulate key aspects of sediment  
89 transport. For example, it is crucial to simulate how the suspended sediment concentration (SSC) that  
90 drives inorganic deposition (i.e., mud) varies in space, such as the SSC decreases with distance from the  
91 channels (Christiansen et al., 2000; Fagherazzi et al., 2012), thus making the marsh interior more  
92 susceptible to entering the pond runaway regime. In addition, lateral sediment redistribution by soil  
93 diffusion (or soil creep), which is present along marsh boundaries with sharp elevation gradients such as  
94 the banks tidal creeks (Kirwan and Murray, 2007; Mariotti, 2018; Mariotti et al., 2019, 2016), could  
95 transfer sediment from high to low elevation areas and thus affect the rate of vertical elevation change.

96 Another important aspect to consider is the biogeochemical dynamics of ponds. The emergent vegetation  
97 that dominates the marsh platform (e.g., *Spartina alterniflora*, *S. patens*, *Distichlis spicata*, etc.) cannot  
98 survive in ponds because of inundation stress or because of the high salinity that results from the absence  
99 of regular flushing (Pethick, 1974). Instead, ponds in New England marshes are colonized by

100 communities of micro- and macro-algae and submerged grasses such as *Ruppia maritima* (Harshberger,  
101 1909; Spivak et al., 2017). The organic matter composition of pond surface sediments reflects inputs from  
102 algal and plant communities that colonize ponds during formation (Spivak et al., 2018). Yet, the  
103 contribution of submerged algae and grasses to vertical accretion in ponds is likely negligible, given that  
104 ponds tend to be net heterotrophic (Spivak et al., 2017) and thus do not accumulate carbon but rather  
105 remove the existing one.

106 In addition to the absence of vertical accretion, ponds might actually experience a net elevation loss.  
107 Indeed, the high rates of respiration, driven primarily by sulfate reduction (van Huissteden and van de  
108 Plassche 1998), convert buried organic matter into dissolved inorganic carbon and thereby contribute to  
109 soil column collapse and pond deepening (Johnston et al., 2003; Spivak et al., 2018, 2017). The elevation  
110 trajectory of ponds is thus diametrically opposite to that of the marsh platform, which gains elevation  
111 through time via suspended sediment deposition and *in situ* plant production. As a result, ponds in New  
112 England marshes are likely experiencing a gradual deepening with respect to the surrounding marsh  
113 platform (Wilson et al., 2009, 2010).

114 Here, we develop a spatially explicit model for pond dynamics. We apply the model to the Barnstable  
115 marsh (MA, USA), which is a typical mesotidal marsh in New England, and constrain the model with  
116 field data and remote sensing analysis. We also consider the case with a smaller tidal range, using as  
117 reference a nearby microtidal marsh with limited sediment supply (the Sage Lot Pond marsh). Then, we  
118 explore the model for different RSLR rates and sediment supply to predict future marsh trajectories. As  
119 suggested by a previous idealized model (Mariotti, 2016), we expect to find a threshold above which  
120 ponds never revegetate and thus lead to permanent marsh loss. By including pond dynamics within the  
121 model, we predict marsh loss when the marsh complex enters the runaway pond regime, which occurs  
122 even when deposition on the vegetated marsh platform is equal or greater than the RSLR rate, a  
123 commonly used threshold for marsh drowning (Morris et al., 2002).

## 124 **2. Site description**

125 The study area is in the New England region of the United States, which experiences a temperate climate,  
126 about 1000 mm of precipitation per year, a growing season from May to September, and overnight freezes  
127 during the winter (Mariotti et al., 2019). Ice rafting has been documented to occur, especially in  
128 concomitance with winter storm surges (Argow et al., 2011).

129 Barnstable is a mesotidal backbarrier marsh, located on the north side of the Cape Cod peninsula (Fig. 1).  
130 The spring tidal range is about 3.6 m (NOAA Sesuit Harbor station 8447241). The marsh is dominated by  
131 *S. alterniflora* in the low marsh and *S. patens* in the high marsh (Redfield, 1972). The majority of the  
132 Barnstable marsh has been ditched since the early 1900s. For simplicity, in this study we focus on an area  
133 that does not have man-made ditches (Fig. 1). This choice allows us to isolate and understand the spatially  
134 explicit pond dynamics under natural conditions, without the confounding effects of mechanical  
135 anthropogenic disturbances.

136 Sage Lot Pond is a polyhaline, microtidal (0.7 m spring tidal range, NOAA Woods Hole Station 8447930)  
137 backbarrier marsh located on the south side of the Cape Cod peninsula (Fig. 1). The marsh is dominated  
138 by short form *S. alterniflora* on the low marsh and *Distichilis spicata*, *Juncus gerardii*, and some *S.*  
139 *patens* at higher elevations (Gonneea et al. 2019). This marsh is also ditched.

140 According to the nearby NOAA station 8443970, mean sea level was -9.2 cm in the NAVD88 datum  
141 during the epoch 1983-2001. Considering the recent increase in sea level, we assume that MSL is now at  
142 0 m NAVD88, which agrees with the datum analysis in the nearby Plum Island Estuary marsh  
143 (Hopkinson et al., 2018).

### 144 **3. Methods**

#### 145 **3.1 Field measurements and remote sensing analysis**

146 For the Barnstable marsh, suspended sediments in tidal creek water were collected in triplicate 1-liter pre-  
147 combusted (450 °C) glass bottles from four different locations (Fig. 1) between June 21<sup>st</sup> and August 1<sup>st</sup>  
148 2018. All samples were collected during the incoming tide. Samples were filtered through pre-combusted  
149 and pre-weighed glass fiber filters (nominal pore size 0.45 µm). The filters were then dried to constant

150 mass (60 °C) and concentrations were calculated by normalizing suspended sediment mass to the volume  
151 filtered. While this sampling is not a comprehensive characterization of the sediment dynamics, it  
152 provides at least a magnitude estimate, which is often the only data available (Cavatorta et al., 2003).

153 Sediment cores were collected from three transects at approximately 2 m (channel adjacent) and 100 m  
154 (marsh interior) from the creek bank (Table 1). All cores were taken in the vegetated platform, i.e., not in  
155 a pond. Cores were collected with a modified piston core where a plastic core liner (11 cm diameter) was  
156 fitted with a gasketed piston and placed on the sediment surface. The core liner was pushed ~70 cm into  
157 the marsh subsurface while the piston was maintained at the surface to minimize compaction, which was  
158 observed through the clear core liner. The cores were split vertically, sampled at 1 cm intervals to 45 cm  
159 below soil surface and 2 cm intervals thereafter, frozen, and then freeze-dried. Sediment samples were  
160 prepared for gamma analysis by sealing approximately 5 g of dried, homogenized peat for 3 weeks, and  
161 counting on a planar-type gamma counter for 24 to 48 hours to measure  $^7\text{Be}$ ,  $^{137}\text{Cs}$ ,  $^{210}\text{Pb}$ , and  $^{226}\text{Ra}$  at  
162 477, 661.6, 46.5 and 352 KeV energies respectively (Canberra Inc., USA). Detector efficiency was  
163 determined from EPA standard pitchblende ore in the same geometry as the samples. Activities of  $^7\text{Be}$ ,  
164  $^{137}\text{Cs}$ , and  $^{210}\text{Pb}$  were decay corrected to time of collection. Suppression of low energy peaks by self-  
165 adsorption was corrected for according to (Cutshall et al., 1983). Excess  $^{210}\text{Pb}$  was calculated by  
166 subtracting supported  $^{226}\text{Ra}$  from total  $^{210}\text{Pb}$  with a detection limit of 0.1 dpm g<sup>-1</sup>. Sediment ages were  
167 calculated using the continuous rate of supply  $^{210}\text{Pb}$  age model, a variant on the advection-decay equation  
168 (Appleby and Oldfield, 1978). This age model assumes that  $^{210}\text{Pb}$  down-core activity is a function of  
169 decay and variable sediment accretion, however, the full  $^{210}\text{Pb}$  profile must be captured to prevent bias  
170 towards ages that are too old and accretion rates that are too low at depth (Binford, 1990). Vertical  
171 accretion rates were calculated as the age difference between each interval, with temporal resolution  
172 typically 2 to 10 years depending on marsh, treatment, and sediment age.

173 Ponds within a few hundred meters from the sites where cores were collected were surveyed in the  
174 summer of 2019 in one of two ways (Fig. 1G). First, 200 marsh-pond boundaries were surveyed in 2019



175 by measuring the elevation of the marsh adjacent to the pond edge and the elevation of the pond bed  
176 adjacent to the pond edge using an RTK-GPS with vertical accuracy of 2 cm. The height of the pond bank  
177 was calculated as the difference between these measurements. Second, elevation transects running  
178 through the diameter of the pond were surveyed for thirteen of the 200 ponds (five small, five medium,  
179 and three large ponds). The absolute bed elevation was referenced to the elevation of the adjacent marsh  
180 surface, which was surveyed with the RTK-GPS.

181 We performed a remote sensing analysis using two datasets: USGS Single Frames Aerial Photos from  
182 March 1973 with resolution of ~0.5 m and USGS high resolution orthoimages from April 2014 with  
183 resolution of 0.075 m, both of which were collected at low tide (earthexplorer.gov). We also used USGS  
184 Lidar collected in 2014 with resolution of 1 m (OCM Partners, 2019). For consistency we resampled all  
185 datasets to a 1 m resolution. In both images we defined isolated ponds as those cells with standing water  
186 at low tide, which were easily identifiable using a threshold on the intensity of the visible band. Pond  
187 cells were clustered together using a five-point stencil connection, such that pond cells that touched each  
188 other either on the top, bottom, right, or left boundary were grouped together. Then, we identified the  
189 same ponds in each image and calculated the rate of area change. We excluded from the analysis those  
190 ponds that either merged together or reconnected to the channel network between 1973 and 2014. From  
191 the rate of area change, we calculated the equivalent rate of pond radius expansion. Change was measured  
192 as a difference in area rather than the retreat of the pond edge, eliminating any error due to image  
193 misalignment.

194 For the Sage Lot Pond marsh, SSC was measured from 2011 to 2018 across all seasons and tides. A total  
195 of 258 grab samples (500 mL each) were collected and stored at 4 °C for a maximum of 1 week and then  
196 filtered through pre-combusted borosilicate glass fiber filters (0.7 um pore size), rinsed thoroughly with  
197 deionized water to remove salts, and dried at 105 °C for >4h. SSC was determined as the ratio of dried  
198 filtrate mass total per sample volume. Existing vertical accretion measurements for Sage Lot Pond marsh  
199 (Gonneea et al., 2019, 2018) are also reported in Table 1.

## 200 **3.2 Model for pond dynamics**

201 Within the model, the pond dynamics is implemented as a cellular automata, in which each cell is  
202 described by its state (which can only take a finite number of values) without explicitly simulating the  
203 elevation. Channels are special cells that are fixed in time, which do not widen, narrow, or migrate  
204 laterally. These cells don't take part in the evolution of the cellular automata and are collectively defined  
205 as "channel network". Cells that are not part of the channel network are marsh cells, which collectively  
206 constitute the marsh domain. Marsh cells are either connected or isolated. Connected cells experience  
207 tidal fluctuations, and are defined as vegetated platform if their elevation is above the lower limit for  
208 vegetation growth ( $z_{min}$ ) or mudflat if their elevation is below ( $z_{min}$ ). Isolated cells, also called isolated  
209 ponds or ponds, do not experience tidal fluctuations or exchange with the channel network. Pond cells  
210 with an elevation below  $z_{min}$  are defined as drowned ponds (Fig. 2).

211 Two processes allow for connected marsh cells to become isolated cells: pond formation and pond  
212 expansion. In the real marsh, formation of new ponds can take place by a variety of mechanisms. A slight  
213 depression in the marsh might lead to water logging and rapid decay of the marsh peat. Deposition of rafts  
214 composed of either eroded plant material or macroalgae might kill the standing vegetation and  
215 temporarily prevent new plant growth (Pethick, 1974). Ice rafting might compress the marsh (Argow and  
216 FitzGerald, 2006) or remove large pieces of standing vegetation. Sub-surface piping might collapse the  
217 marsh from below (Kesel and Smith, 1978). Large patches of vegetation can be removed by grazers such  
218 a geese herbivory (Kirwan et al., 2008) and major storms (Howes et al., 2010). Rather than explicitly  
219 modeling these different mechanisms, we simply assume that individual ponds form at a constant rate  $k_{seed}$   
220 [#ponds/m<sup>2</sup>/yr], that is, during each time step  $\Delta t$ , each vegetated marsh cell is transformed into a pond cell  
221 with a probability  $k_{seed}\Delta t\Delta x^2$ . Pond expansion allows existing ponds (i.e., clusters of connected pond cells)  
222 to enlarge. This process is implemented at every boundary between a pond cell and a vegetated cell.  
223 Expansion is simulated using a probabilistic approach (Mariotti and Canestrelli, 2017), in which a

224 vegetated cell adjacent to a pond cell is converted to a pond cell with a probability  $p=k_{exp}\Delta t/\Delta x$ , where  $k_{exp}$   
225 is the expansion rate [m/yr].

226 Pond cells transform into vegetated cells though pond drainage. In the real marsh, pond drainage occurs  
227 when a pond become close enough to the channel network that a new connecting channel forms, as  
228 exemplified in Fig. 1E. Then, the pond fills in quickly (assuming that there is enough sediment supply)  
229 and the connecting channel, now lacking the tidal prism associated with the pond, eventually silts in. The  
230 model is unable to explicitly simulate the formation or closure of these transient connecting channels,  
231 since the model does not simulate tidal hydrodynamics and the main channel network is assumed to be  
232 fixed in time. We thus parameterize this effect by assuming that pond drainage instantaneously occurs  
233 when a connected cell becomes closer than a critical distance  $L$  from the channel network. When this  
234 happens, the whole pond, which consists of all pond cells that are contiguous to at least one pond cell  
235 with distance  $L$  from the channel network, are drained and all its cells become connected cells. The  
236 distance  $L$  is the distance at which the pressure gradient generated by the water in the pond is able to start  
237 scouring the marsh soil – possibly by seepage and piping first – and eventually form a connecting  
238 channel. In theory this distance might be calculated using a hydrodynamic and sediment transport model,  
239 but for simplicity this distance is calibrated to reproduce the observation that ponds tend to drain when  
240 they get about 20 m away from the main channel network (Fig. 1E).

### 241 **3.3 Model for elevation dynamics**

242 The elevation of each marsh cell relative to mean sea level,  $z(x,y,t)$ , is described as

$$243 \quad \frac{dz}{dt} = D_p + D_m - S - P - R \quad (\text{Eq. 1})$$

244 where  $D_p$  is the *in situ* organic accretion by marsh plants,  $D_m$  is the accretion from suspended sediment,  
245 which we assume is composed of mud and thus transported in suspension,  $S$  is the divergence of the creep  
246 flux  $F$ ,  $P$  is the elevation loss by pond dynamics (which is further explained below), and  $R$  is the relative  
247 sea-level rise rate.

248 The organic accretion by *in situ* plant production is  $D_p = D_{pMAX}B$ , where  $D_{pMAX}$  is the maximum accretion  
 249 rate [mm/yr] and  $B$  is a function that describes the dependence on the bed elevation and serves as a proxy  
 250 for the hydroperiod,  $B = \max[0, 4(z - z_{min})(z_{max} - z)/(z_{max} - z_{min})^2]$ , where  $z_{min}$  and  $z_{max}$  are the  
 251 minimum and maximum elevation for vegetation growth.  $B$  is set equal to zero in isolated ponds,  
 252 simulating the absence of marsh plants and assuming that any macrophytes and microphytobenthos  
 253 present in ponds do not contribute to substantial vertical accretion.

254 Mud accretion depends on hydroperiod and the local SSC. The spatial pattern of SSC is described by

$$255 \quad C = C_o(\alpha + (1 - \alpha)e^{-\beta l}) \quad (\text{Eq. 2})$$

256 where  $C_o$  is the time-average suspended sediment concentration in the channels,  $l(x,y)$  is the distance to  
 257 the closest cells that belong to the channel network,  $\beta$  is the decay factor for SSC with distance from the  
 258 channel network, and  $\alpha$  is the factor describing the SSC that is spatially uniform. This last parameter  
 259 allows transport of sediment even to large distances from the channels, and thus can parameterize  
 260 processes such as storm-induced deposition on the marsh platform. Mud accretion thus equals

$$261 \quad D_m = \frac{C \min(h, r) \min(1, h/\Delta r)}{T \rho_m} \quad (\text{Eq. 3})$$

262 where  $h$  is the depth with respect to MHHW,  $T$  is the tidal period,  $\rho_m$  is the dry bulk density of the mud,  
 263 and  $\Delta r$  is the difference between the spring and neap high tide. The last factor in the numerator is  
 264 introduced to account for modulation introduced by the spring-neap variability. If the marsh elevation is  
 265 at least  $\Delta r$  lower than MHHW, the marsh is inundated every tidal cycle and this factor is equal to one. If  
 266 the marsh is higher than this elevation, the marsh is only inundated during spring tides, and the factor will  
 267 be less than one. This allows mud to deposit at high marsh elevations but at a lower rate.

268 In theory, ponds could accrete vertically by suspended sediment deposition akin to the marsh platform.

269 Yet, several reasons suggest that this deposition is small. First, despite ponds having a large depth, the  
 270 water in the pond is not exchanged during tides. Only the thin layer of water that flows over the pond

271 should count toward sediment deposition as formulated in Eq. 3 (which assumes that the water depth is  
272 equal to the depth of the flow that floods that cell). Second, ponds lack the emergent marsh vegetation  
273 that enhances sediment trapping. As a consequence, for the same water depth and sediment concentration,  
274 a vegetated pond should experience a lower sediment deposition than a vegetated marsh. Third, ponds are  
275 generally far from channels, specifically they are always farther than the distance  $L$ . As such, the  
276 suspended sediment concentration above ponds is always lower than on the marsh close to the channel  
277 edge. Furthermore, field data suggested that ponds in a New England salt marsh are isolated from the tidal  
278 network and do not import sediment (Spivak et al., 2017). Overall, sediment deposition in the ponds is  
279 likely very small, and for simplicity is set equal to zero.

280 The creep flux  $F$  parameterizes all processes that cause soil diffusion and is set equal to  $\mu\nabla z$ , where  $\mu$  is  
281 the soil diffusivity coefficient, whose value was empirically found equal to  $\sim 0.1$  m<sup>2</sup>/yr (Mariotti et al.,  
282 2019). The creep flux is set equal to zero within ponds and, more importantly, at the pond edges. This  
283 choice reflects the absence of tidal oscillations, a process that creates “tidal fatigue” and is responsible for  
284 the fast creep in channel banks (Mariotti et al., 2019). This is due to the standing water in the isolated  
285 ponds maintaining hydrostatic pressure on the pond bank and preventing slumping during low tide. Thus,  
286 the model allows isolated ponds to have relatively steep banks, as observed in the field (Wilson et al.,  
287 2010). When pond cells reconnect, they drain instantaneously, and creep can take place. Excluding the  
288 creep process at the edge of isolated ponds results in isolated pond expansion only occurring according to  
289 the pond expansion term  $k_{exp}$ , which can be calibrated by direct comparison with the observed historical  
290 expansion rate of isolated ponds. To summarize, creep does not affect isolated pond dynamics, but does  
291 affect the dynamics of mudflats (i.e., connected ponds) and prevents the formation of an unrealistically  
292 large elevation gradient in the marsh interior, which in reality might have been smoothed by  
293 hydrodynamic processes other than creep but that the model is unable to explicitly simulate.

294 The channel dynamics is not explicitly simulated, and the channel elevation is kept equal to the lower  
295 limit for vegetation growth. This elevation acts as a boundary condition for the bed elevation gradients

296 and thus affects the sediment creep flux near the banks. Noticeably, creep from the marsh platform into  
297 the channels moves material out of the marsh domain and thus acts as a sink. Creep can also redistribute  
298 sediment within the marsh domain; this does not count as either a sink or source because it conserves  
299 sediment.

300 Finally, the term  $P$  includes the platform elevation loss through pond processes. When a connected cell  
301 becomes a pond cell by either pond formation or pond expansion, it loses the elevation  $Y = \min(Y_{max},$   
302  $\max(0, z - z_{min}))$ , where  $Y_{max}$  is the maximum scour thickness, calibrated with field data, and  $z_{min}$  is the  
303 lower elevation limit below which pond scour does not occur.  $Y$  is the thickness of the material that is  
304 instantaneously removed from the system, such that the elevation  $z$  is lowered by the amount  $Y$ .

305 The term  $P$  also includes pond deepening, which simulates organic matter decomposition via sulfate  
306 reduction in the bed of the pond. Pond deepening is set equal to a constant rate ( $P_{deepening}$ ) if  $z > z_{min}$  and to  
307 zero if  $z < z_{min}$ . Even though we introduced active pond deepening to simulate the loss of elevation caused  
308 by organic matter decomposition, this term could be more generally considered as the net effect of all the  
309 processes that change pond elevation. For example, if we assume that some sediment settles in the pond  
310 during high tide, the term  $P_{deepening}$  should be interpreted as the net deepening, including the actual pond  
311 deepening by organic matter decomposition minus the elevation gain caused by sediment deposition. If  
312 sediment deposition was larger than organic matter decomposition,  $P_{deepening}$  could be negative, and the  
313 pond might gain elevation through time. Given that this parameter is calibrated by comparing measured  
314 and modeled pond depths, not by directly measuring the deepening or accretion, we are unable to isolate  
315 these two components.

316 To summarize, the pond depth, relative to the surrounding marsh platform, is controlled by three  
317 mechanisms: 1) the initial scour, which takes place by either pond formation or expansion, 2) the active  
318 pond deepening, and 3) the relative deepening caused by the surrounding marsh gaining elevation through  
319 organic and inorganic accretion.

### 320 **3.4 Coupling between pond dynamics and elevation dynamics**

321 As outlined above, the bed elevation is affected by pond processes of formation, expansion, and  
322 deepening through the term  $P$  (Eq. 1). While the cellular automata model formulated in Section 2.2 is  
323 independent of bed elevation, the elevation dynamics is introduced by allowing ponds to form and expand  
324 only in vegetated marsh cells. This rule keeps ponds from forming and expanding into a mudflat, which is  
325 defined as a connected cell with an elevation lower than  $z_{min}$ . This model implementation is a result of  
326 only allowing the processes associated with isolated pond formation and expansion to occur in highly  
327 organic soil that can be oxidized and compressed.

328 If the pond elevation at the time of drainage is higher than  $z_{min}$ , the pond revegetates just after it is  
329 drained. In other words, the cell instantaneously switches from a pond to a vegetated marsh status. In this  
330 scenario, every cell that is not a pond is a vegetated marsh that can be transformed back to a pond through  
331 either pond formation or pond expansion. In this case, the pond dynamics without elevation is equivalent  
332 to the pond dynamics with elevation, so the cellular automata can be run independently of the elevation.

333 On the other hand, if the connected ponds do not revegetate immediately, they become mudflat cells in  
334 which ponds are not allowed to form (because  $z < z_{min}$ ). These areas affect the dynamics of pond formation  
335 and expansion, and thus the cellular automata model needs to be run together with the elevation model.

336 A special consideration should be given to cells whose elevation drops below the vegetation limit  $z_{min}$ .  
337 These cells can be either drowned ponds or mudflats (Fig. 2). Neither has organic accretion by vegetation  
338 (Eq. 3), but only the mudflat cells receive inorganic sediment and are allowed to creep under the model  
339 specifications. If a drowned pond is surrounded by mudflats, the pond cannot expand. As a result,  
340 drowned ponds will never intercept a channel and will never drain in the model domain. In reality,  
341 drowned ponds should connect to the channel network through channels that quickly form in the  
342 mudflats, but these are not explicitly simulated in the model. Connecting these drowned ponds to creeks  
343 will not immediately allow for pond revegetation since the pond is still below the vegetation limit, but it  
344 will allow for inorganic accretion and creep, which will both increase the bed elevation and potentially  
345 allow for revegetation. In the model we account for this dynamic by introducing the rule that any drowned

346 pond that touches a mudflat becomes a mudflat itself, and receives inorganic sediment. Then, the  
347 evolution of the mudflat would follow the elevation dynamics as previously described.

348 To summarize, the pond dynamics can be affected by the presence of mudflat cells, since ponds cannot  
349 form or expand into these cells. The formation of mudflats is controlled by active pond deepening  
350 ( $P_{deepening}$ ) and by RSLR; the recovery of mudflats is controlled by mud accumulation and by RSLR (Fig.  
351 2). If the amount of mudflats at any time is negligible (a few percent of the total marsh area), then the  
352 elevation dynamics would in practice not affect the pond dynamics.

## 353 **4. Results**

### 354 **4.1 Field measurements**

355 The pond expansion rate, calculated using remote sensing, was equal to  $\sim 1.5$  cm/yr, with a weak  
356 dependence on the pond size (Fig. 3). This is calculated for ponds that did not merge between 1973 and  
357 2014 and thus only includes ponds smaller than about 20 m. We were not able to measure expansion for  
358 larger ponds. Detailed transects across thirteen ponds indicate that ponds are 0.3-1.2 m deep and that their  
359 depth increases with diameter. The survey of 200 marsh-pond boundaries revealed that the depth of the  
360 pond immediately adjacent to the bank was  $0.46 \pm 0.21$  m. As such, the depth of the pond close to the edge  
361 is relatively uniform, whereas the depth in the middle of the pond has a greater variability. Field  
362 measurements at Barnstable marsh show an accretion of  $4.6 \pm 2.5$  mm/yr near the channel and  $5.1 \pm 3.3$   
363 mm/yr in the marsh interior over the past 100 years (Table 1). Total suspended sediment concentrations  
364 were  $29.3 \pm 3.6$  mg/l for Barnstable and  $5.0 \pm 2.8$  mg/l for Sage Lot pond.

### 365 **4.2 Pond dynamics not coupled to elevation**

366 The model simulations were run in a portion of the Barnstable marsh about 1.2 x 1.2 km (Fig. 1C). Using  
367 the 2014 Lidar topography, the channel network was defined as the area with an elevation lower than the  
368 limit for vegetation growth, which was assumed to be equal to MSL. Areas that were identified as ponds  
369 (Section 2.1) were excluded from the channel network.



370 The pond model is first run without including the requirement that ponds can only form and expand  
371 where the marsh elevation is greater than  $z_{min}$ . In this case, the pond dynamics does not depend on bed  
372 elevation. This simplification is equivalent to the fully coupled model if the pond elevation never drops  
373 below  $z_{min}$ , and it is nearly equivalent to the fully coupled model if the amount of mudflats is negligible,  
374 which is the case if mudflats recover quickly. The advantage of running the model without the elevation  
375 dynamics is to emphasize a key feature of pond dynamics, that is, the spatial distribution of ponds does  
376 not depend on RSLR and sediment supply. As such, the parameters for pond evolution ( $k_{seed}$  and  $k_{exp}$ ) can  
377 be calibrated against observations without being affected by the uncertainties associated with RSLR (and  
378 its variability during the last century) and sediment supply (which is estimated using a limited number of  
379 samples).

380 Starting with a marsh without ponds, we run the model for 1000 years to reach a steady state, defined as  
381 the period in which the time-averaged statistical distribution of ponds does not change. We found that  
382 pond dynamics does not depend on the size of the ponds formed via the seeding mechanism, rather the  
383 same steady state pond distribution is obtained if the ponds formed by the seeding mechanism are  
384 composed of a single or several cells (and thus the initial ponds is larger). This occurs because the amount  
385 of pond area created by seeding, where ponds are introduced into the model, is small compared to the area  
386 gained by pond expansion. As such, the main effect of pond formation is not to directly increase the pond  
387 area, but rather to create “seeds” that allow for pond expansion. This also confirms that pond formation  
388 should have units of  $\#ponds \cdot m^{-2} yr^{-1}$  and not of  $m^2 m^{-2} yr^{-1}$ .

389 We found that the steady state pond size distribution only depends on the ratio between pond formation  
390 and expansion rates. This is confirmed by noticing that the ratio between the two rates has units of  
391  $\#ponds/m^3$  and is independent of time. The actual values of the rates only affect the time needed to reach  
392 the steady state distribution. The ratio between pond formation and expansion rate that best fits the pond  
393 size distribution (Fig. 4) is  $0.027 \#ponds/m^3$ . If the ratio decreases, the number of small ponds decreases  
394 while allowing for only a few large ponds (Fig. 4). Intuitively, in this scenario each pond has more time to

395 expand before eventually being drained. Using the measured pond expansion rate (1.5 cm/yr), the pond  
396 formation rate is estimated to be  $4 \cdot 10^{-4}$  ponds $\cdot$ m<sup>2</sup> $\cdot$ yr<sup>-1</sup>. We could not directly measure this rate because of  
397 the difficulty of detecting small ponds.

### 398 **4.3 Elevation dynamics**

399 Simulations that include the elevation dynamics (Section 2.3) are run for 1000 years, in which the first  
400 900 years have  $R$  of 1 mm/yr and the last 100 years have  $R$  of 2.9 mm/yr, thus representing the RSLR  
401 acceleration in the 19<sup>th</sup> century (NOAA Woods Hole Station 8447930). Thus, year 900 of the simulation  
402 roughly corresponds to year 1914, whereas year 1000 roughly corresponds to year 2014 (i.e., present  
403 time). The model at year 0 is initialized with an elevation equal to the 90<sup>th</sup> percentile of the vegetation  
404 range, i.e.,  $0.9(r/2)=1.62$  m. Despite this initialization of marsh elevation being arbitrary, it does not affect  
405 the results after about 500 years. Put differently, any initial marsh elevation would lead to the  
406 (statistically) same results during the last few hundred years of the simulation. As such, this approach  
407 recreates a synthetic marsh representative for the beginning of the 20<sup>th</sup> century that is 1) at steady state  
408 according to the processes included in the model, 2) independent of any arbitrary initial marsh elevation,  
409 3) independent of any topography measured at present time. Specifically, the measured Lidar is not used  
410 to initialize the marsh elevation nor the pond distribution. Only the geospatial distribution of channels  
411 (which could be reconstructed from aerial images without elevation) is needed to initialize the model.  
412 First, we consider the elevation dynamics without the presence of ponds (Fig. 5). We analyze this  
413 scenario by considering the spatially averaged vertical fluxes over the marsh domain (Fig. 6). As  
414 expected, the net vertical accretion is equal to the RSLR rate. When RSLR rate increases to 2.9 mm/yr,  
415 the net vertical accretion lags behind, but it nearly matches the RSLR rate after about 100 years (i.e., at  
416 present times). The gross vertical accretion at present times is 5.1 mm/yr. This value represents the  
417 spatially averaged accretion rate; in reality the accretion is much higher in the marsh adjacent (<10 m) to  
418 channels, where it can be up to 20 mm/yr (Figs. 5, 7C). This additional accretion is balanced by bank  
419 creep, which transports sediment out of the marsh domain. When spatially averaged over the entire marsh,

420 this creep flux creates an equivalent deficit of 2.2 mm/yr, which allows the net vertical accretion to  
421 balance the RSLR rate (Fig. 6).

422 Next, we run the model including the mechanisms of pond formation, expansion, and deepening. The  
423 maximum initial pond depth  $Y_{max}$  (which is both the maximum initial scour of new ponds, as well as the  
424 maximum initial scour when the pond edge expands) is set equal to the measured height of the pond edge,  
425 which was measured for Barnstable marsh to be 0.46 m. The consequences of this choice in the model are  
426 that 1) small ponds would have a nearly uniform depth across the pond, and that depth would be about  
427 0.46 m, 2) larger ponds would have a depth greater than 0.46 m in their center, which is older and thus  
428 may have deepened over time due to organic matter decomposition as well as accretion of the adjacent  
429 marsh platform, whereas their edges, which formed recently, would have a depth of ~0.46 m. The active  
430 pond deepening  $P_{deepening}$  was instead calibrated to match the observed depth in the middle of the ponds  
431 (Fig. 8). As expected, the pond depth is much greater in the middle than at the edge, and the depth in the  
432 middle of the pond increases with the pond diameter.

433 Ponds do not affect the marsh dynamics in the buffer zone close to the channel network, where ponds are  
434 drained instantaneously. This is equivalent to assuming that they do not form at all and cannot expand. As  
435 such, the model that includes pond dynamics has a similar pattern of bank creep and excess accretion on  
436 the marsh adjacent to the channel as the model without pond dynamics (Fig. 6). On the other hand, ponds  
437 drastically change the dynamics of the marsh interior. Ponding creates a heterogeneous landscape, with  
438 low elevation areas surrounded by high marsh areas. This elevation pattern is mirrored by a spatially  
439 heterogeneous vertical accretion, where the net vertical accretion in ponds is zero (if not negative,  
440 because of active pond deepening), whereas recently connected ponds experience enhanced vertical  
441 accretion. Compared to the case without ponds, the average marsh elevation is also lower.

442 Because pond reconnection is a stochastic process, the vertical accretion rate is not constant in time. In  
443 particular, there are periods when large ponds are drained and the vertical accretion suddenly increases  
444 (Fig. 6). Over a sufficient time period (e.g. 50 years), however, the net vertical accretion rate is equal to  $R$ .

#### 445 **4.4 Exploring the effects of RSLR rate, sediment supply, and tidal range**

446 To generalize our results, we perform a series of explorative simulations with different sediment supplies  
447 ( $C_o$ ), RSLR rates ( $R$ ), and tidal ranges ( $r$ ). In order to consistently initialize the simulations, we start with  
448 a uniform elevation equal to  $0.9(r/2)$  with no ponds, and then run the model with  $R$  equal to 1 mm/yr for  
449 500 years, which is enough to establish a steady state pond distribution (Fig. 6). As already pointed out,  
450 the choice of the initial elevation does not affect the results after about 500 years. After 500 years, we  
451 changed a single parameter (either  $R$  or  $C_o$ ) while keeping all the other parameters fixed, and run the  
452 simulations for an additional 1000 years (Fig. 9). We focused on scenarios in which the vegetated marsh  
453 kept pace with RSLR and thus all marsh loss is due to pond expansion.

454 First, we consider the effects on increasing  $R$  or decreasing  $C_o$  in a mesotidal marsh such as Barnstable  
455 marsh. For the relatively high sediment supply of Barnstable marsh ( $C_o=30$  mg/l), the RSLR rate does not  
456 affect the dynamics of ponds, which always occupies  $\sim 10\%$  of the marsh. For the case with a lower  $C_o=10$   
457 mg/l, lower  $R$  gives nearly identical results as for the case with a higher  $C_o$ , with pond area remaining at  
458  $\sim 10\%$  of the total marsh area, whereas high  $R$  starts to affect pond area (Fig. 9A). For example, for  $C_o=10$   
459 mg/l and  $R=8$  mm/yr, the total unvegetated area (ponds plus mudflats) increases to about 25% within 500  
460 years (Fig. 9A). Noticeably, under these conditions, the unvegetated area stabilizes and does not increase  
461 indefinitely even after 1000 years.

462 Next, we consider the case of a marsh with a smaller tidal range. We use as a reference Sage Lot Pond  
463 marsh, which has a spring tidal range of 0.7 m ([Gonneea et al. 2019](#)). Field measurements indicate that  
464 this marsh has a small sediment supply equal to 5 mg/l. For simplicity, we consider the same channel  
465 geometry as of Barnstable marsh but with a smaller tidal range. Accordingly, we modify the vegetation  
466 limit, the initial marsh elevation, the maximum initial pond elevation, and the spring-neap variability  
467 (Table 2). For the microtidal case, we found that for low  $R$  the unvegetated area is still  $\sim 10\%$ , but for  
468 higher rates the unvegetated area increases quickly, and can be up to 100%, indicating loss of the entire

469 the marsh platform (Fig. 9B). The model predicts that the marsh would enter the pond runaway regime for  
470  $R \sim 3$  mm/yr (Fig. 9B).

471 We also compared the model predictions with the measured accretion rates in Barnstable and Sage Lot  
472 Pond marsh. We separated the spatially averaged accretion predicted by the model between the marsh  
473 adjacent to channels (less than 10 m from the nearest channel, which roughly coincides with the low  
474 marsh, and is about 29% of the total marsh area) and the marsh interior (more than 10 m from the nearest  
475 channel, where bank creep is virtually zero, and is about 71% of the total marsh area). For a marsh with  
476 low tidal amplitude and sediment supply such as Sage Lot Pond, the model predicts that when RSLR rate  
477 was 1 mm/yr, the gross vertical accretion rates was  $\sim 2.6$  mm/yr in the marsh adjacent to channels and  
478  $\sim 1.4$  mm/yr for the marsh interior (Fig. 7B). After the acceleration in RSLR to 2.9 mm/yr the model  
479 predicts that the gross vertical accretion increases to  $\sim 4.1$  mm/yr in the marsh adjacent to the channels and  
480 to  $\sim 3$  mm/yr in the marsh interior (Fig. 7B). For comparison, the field measurements of accretion over a  
481 100 year period, which includes the period during modern RSLR acceleration, indicate an accretion rate  
482 of  $3.7 \pm 2.0$  mm/yr close to the channels and  $1.4 \pm 0.3$  mm/yr in the interior (Table 1). For the Barnstable  
483 marsh, with a higher tidal range and sediment supply, the model predicts gross vertical accretion rates of  
484  $\sim 9.5$  mm/yr near channels and  $\sim 2.8$  mm/year in the marsh interior when RSLR rate is 1 mm/yr, and  $\sim 11.5$   
485 mm/yr near channels and  $\sim 4.0$  mm/year in the marsh interior when RSLR rate is 2.9 mm/yr (Fig. 7A). For  
486 comparison, field measurements at Barnstable marsh show an accretion of  $4.6 \pm 2.5$  mm/yr near the  
487 channel and  $5.1 \pm 3.3$  mm/yr in the marsh interior over the past 100 years.

488 As an indicator of the overall marsh status, we calculated the spatially-averaged primary productivity  
489 normalized by the maximum productivity (Fig. 9). The productivity of the vegetated marsh depends on  
490 the bed elevation following the function  $B$  (section 3.3), whereas the productivity in the ponds is equal to  
491 zero. As the RSLR rate increases, the marsh elevation decreases and thus the productivity increases. As  
492 the unvegetated pond area starts to increase, however, the overall marsh productivity starts to decrease.  
493 This is particularly evident for the Sage Lot Pond marsh for a RSLR rate greater than 4 mm/yr (Fig. 9B).

494 Finally, we expanded these simulations by systematically considering different tidal ranges (0.7, 1.6, 3.6  
495 m), RSLR rates (1 to 8 mm/yr), and sediment supply concentrations (5 to 30 mg/l) (Fig. 10). We found  
496 that, for small tidal ranges, the rate of marsh loss by pond expansion is highly sensitive to the RSLR rate.  
497 When the RSLR rate increases to 3 mm/yr, marsh loss occurs but is relatively slow, and the amount of  
498 unvegetated area (which includes both ponds and mudflats) increases from 10% to 15% of the total marsh  
499 area during the first 100 years (Fig. 9). A further increase in the RSLR rate (5 mm/yr) drastically  
500 increases the rate of marsh loss, with the amount of unvegetated area increasing from 10% to 40% of the  
501 total marsh area during the first 100 years.

## 502 **5. Discussion**

### 503 **5.1 The pervasive effect of ponds in salt marshes**

504 Ponds in Barnstable marsh expand at a very slow rate (1.5 cm/yr) compared to exposed marsh creekbank  
505 edges that retreat by wave-induced erosion (0.5-10 m/yr) (Elsey-Quirk et al., 2019; Hopkinson et al.,  
506 2018; Leonardi et al., 2016; Marani et al., 2011). Yet, ponds are numerous and collectively have a long  
507 perimeter, and thus are able to affect nearly the entire marsh surface on millennial time scales.

508 Considering an average unchanneled length of 50 m (Marani et al., 2003), a pond formed in the middle of  
509 the marsh would take ~2000 years to reach an area influenced by channel network and drain. Since some  
510 ponds form closer to the channel network initially, 2000 years is likely an upper estimate of the time  
511 needed to reconnect ponds to the channel network and drain. In addition, ponds that merge together will  
512 drastically reduce the time needed for a pond to reconnect to the channel network.

513 Given that the Barnstable marsh is ~4000 years old (Redfield, 1965), we expect that any point on the  
514 marsh was at least once a pond. Indeed, stratigraphic evidence of ponds were found in nearly all cores  
515 taken in a New England salt marsh (ME, USA) (Wilson et al., 2009). However, many historical records  
516 within salt marshes only extend ~100 years, due to age model constraints of the commonly used lead-210  
517 methods, and thus may miss some of these millennial scale dynamics. In any case, the assumption of  
518 steady state marsh accretion often used while interpreting the sedimentary record (Morris et al., 2016)

519 should be evaluated, since even if RLSR rate and sediment supply are constant, a specific site within the  
520 marsh may not be at steady state at any given time due to pond dynamics.

521 Another consequence of pond dynamics is that recently connected ponds (as identified in Fig. 1E) are a  
522 common feature and should be interpreted as part of the basic marsh dynamics as opposed to an indicator  
523 of changes in boundary conditions. Thus, ponds do not necessarily indicate an acceleration in RSLR or  
524 other anthropogenic modifications, but are rather a natural occurrence within many salt marshes. Ponds  
525 also create diverse habitats and ecological niches for wildlife (Brush et al., 1986), and thus should not  
526 necessarily be considered a negative feature within salt marshes.

## 527 **5.2 Vertical accretion in the pond recovery regime**

528 When the marsh is in the pond recovery regime, pond dynamics in the marsh interior increased the  
529 spatially-averaged gross vertical accretion by 0.5-2 mm/yr (Fig. 7), a result that was previously predicted  
530 (Kirwan et al., 2008). This excess accretion is larger for larger tidal ranges, because marshes with a larger  
531 tidal range have a thicker soil profile that can be removed by the ponding processes. Ponding also results  
532 in highly heterogeneous accretion across the marsh platform (Fig. 5), and thus the excess accretion rate  
533 during pond recovery could locally be much higher than 2 mm/yr. For example, the model predicts that  
534 recovering ponds might have accretion rates up to 20 mm/yr (Fig. 5). Indeed, Wilson et al., (2014)  
535 reported vertical accretion rates of 8 mm/yr in recently recovered ponds in a New England salt marsh,  
536 despite the fact that the sediment supply in that marsh was extremely low (~5 mg/l). The model predicts  
537 that the excess accretion rate persists from when a pond revegetates until it reaches the equilibrium  
538 elevation with the marsh surface. In other words, ponds that were drained centuries ago might not have  
539 fully equilibrated and thus might still accrete slightly faster than the RSLR rate. These predictions are  
540 consistent with the 5.1 mm/yr vertical accretion measured in the marsh interior of Barnstable marsh  
541 during a period when relative sea-level rise rate was 2.9 mm/y (NOAA Woods Hole Station 8447930)  
542 (Table 1).

543 Our model also predicts channel bank creep causes an equivalent elevation drop of  $\sim 2$  mm/yr when  
544 averaged over the whole marsh platform (Fig. 6,7). This loss is balanced by an excess vertical accretion  
545 (Mariotti et al., 2016), which can be observed by the gross vertical accretion rate being much larger than  
546 the RSLR rate. Contrary to ponding, this bank creep is localized to the low marsh immediately adjacent to  
547 channels, where the excess vertical accretion can be an order of magnitude higher than RSLR rate (i.e., up  
548 to 20 mm/yr, Fig. 5). This prediction is consistent with the larger vertical accretion rates measured on the  
549 marsh adjacent to channels than on the marsh interior at Sage Lot Pond marsh (Table 1). For Barnstable  
550 marsh, the model predicts that the vertical accretion on the marsh adjacent to channels is  $\sim 11$  mm/yr (Fig.  
551 7A), which is much larger than the measured  $4.6 \pm 2.5$  mm/yr (Table 1). One possible explanation is that  
552 the channel-adjacent area in the model integrates portions of the marsh that are extremely low (e.g., the  
553 vegetated bank located a few meters from the channel). These low areas have a disproportionately high  
554 excess accretion (Fig. 5 and Fig. 7C,D) and strongly influence the average value over the area here  
555 defined as channel-adjacent ( $< 10$  m from the channel network). Field measurements in the channel-  
556 adjacent area, in contrast, are generally taken a few meters inland from the edge of the marsh, with a  
557 higher elevation than the slumping blocks and where the excess accretion is much lower. Indeed, the  
558 cores in Barnstable collected  $\sim 2$  m from the marsh edge are actually  $\sim 5$  m from the lowest vegetated point  
559 (Fig. 1H). Noticeably, the model predicts a minimum in vertical accretion, equal to about 3 mm/yr,  
560 located between 5 and 20 m from the channel (Fig. 7C). This is the region where neither bank creep nor  
561 ponding are present, and thus the gross accretion rate matches RSLR rate.

562 The model also recreates the lagged vertical accretion that follows the acceleration in RSLR rate, a  
563 disequilibrium effect has been previously identified with simplified marsh models (Kirwan and  
564 Temmerman, 2009; Kirwan and Murray, 2008). This lag should be present in every salt marsh that  
565 experienced accelerated RSLR, regardless of pond occurrence or the influence of bank creep.

566 To summarize, the model is able to combine three previously identified mechanisms by which vertical  
567 accretion rates deviate from the RSLR rate, emphasizing that a direct comparison between vertical



568 accretion and RSLR rate can be misleading at best, and overly optimistic for projecting marsh elevation  
569 trajectories.

### 570 **5.3 Vertical accretion in the pond runaway regime**

571 The simple lumped model (Mariotti, 2016) identified the minimum unvegetated accretion,  
572  $D_{cr}=C\cdot r/(2T\cdot\rho_m)$ , as the threshold between pond recovery and pond runaway regimes. Because  $C$  is not  
573 spatially uniform,  $D_{cr}$  varies among the domain.  $D_{cr}$  is lowest in the marsh interior, where

$$574 D_{cr}=\alpha\cdot C_o\cdot r/(2T\cdot\rho_m).$$

575 For  $R<D_{cr}$ , the lumped pond model predicts that every pond recovers. Indeed, the spatially explicit model  
576 predicts that, for any RSLR rate lower than  $D_{cr}$ , ponds always occupy ~10% of the marsh area (Figs.  
577 9,10). This prediction agrees with the finding that stable salt marshes are associated with an unvegetated-  
578 vegetated ratio of ~0.1 (Wasson et al., 2019) (a pond area of 10% corresponds to an unvegetated-  
579 vegetated ratio of 0.11). As for the lumped model, the spatially explicit model predicts an increase in the  
580 total unvegetated area as  $R>D_{cr}$ . The spatially explicit model provides more information than the lumped  
581 model, and specifically predicts that the rate at which marsh loss by pond expansion takes place strongly  
582 increases as  $R$  further exceeds  $D_{cr}$ . Put differently, when  $R$  is just slightly above  $D_{cr}$ , the rate of marsh loss  
583 by pond expansion is extremely low, and the marsh could last thousands of years. On the other hand, once  
584 the threshold for pond runaway is exceeded, even small increases in  $R$  could have catastrophic  
585 consequences for marsh loss.

586 Using  $D_{cr}$  as the threshold for the pond runaway regime is further complicated by the presence of creep,  
587 which can take place at the edge of mudflats (i.e., connected ponds). Creep transfers sediment from high  
588 to low elevations, and thus tends to increase vertical accretion in the mudflats and to lower vertical  
589 accretion on the vegetated platform. For example, a very small mudflat might recover even if  $R$  is slightly  
590 larger than  $D_{cr}$  (which explains why the Sage Lot Pond marsh does not enter the pond runaway regime for  
591  $R=1$  mm/yr even if  $D_{cr}=0.6$  mm/yr). Lateral transport of sediment not associated with creep, including  
592 sediment transport by waves or sheet flow over the marsh, might slightly alter the predictions purely

593 based on vertical accretion rates. Nonetheless, the parameter  $D_{cr}$  captures the transition to the pond  
594 runaway regime within an uncertainty of about 1 mm/yr (Fig. 10).

#### 595 **5.4 Pond formation**

596 A crucial parameter in the model is the rate of pond formation. If ponds do not form, neither the pond  
597 recovery nor the pond runaway regime occurs. In this case, the marsh is either fully vegetated or  
598 disappears by drowning, and thus the marsh landscape is dramatically different than what simulated in our  
599 model (Fig. 5). As such, it is noteworthy to emphasize that ponds are not always present in salt marshes.  
600 Ponds have been identified in the Mid-Atlantic and New England Coast of the USA (Adamowicz and  
601 Roman, 2005; Mariotti, 2016; Schepers et al., 2017) as well as in the northern Gulf of Mexico (Mariotti,  
602 2016; Nyman et al., 1994). Yet, marshes in the South-Atlantic Coast of the USA, including sites with  
603 relatively little human modifications such as in Virginia and Georgia, seem to have few ponds if any at  
604 all. For marshes in which ponds are not common, it is possible that either ponds do not form at all or that  
605 the pond formation rate (the parameter  $k_{seed}$ ) is extremely low. In this latter case the model would predict  
606 that the number of ponds would be highly reduced (Fig. 4) and that their size distribution would be highly  
607 skewed towards a few large ponds.

608 In this study, we assumed that ponds form without explicitly simulating the mechanisms that lead to pond  
609 formation in the first place. In particular, we did not investigate whether the rate of pond formation  
610 changes as a function of environmental drivers. We can only speculate that pond formation might be  
611 related to disturbances related to climate via ice rafting and scour, excessive wrack accumulation,  
612 grazing/bioturbation such as by *Sesarma reticulatum* crab or burrowing species such as fiddler crabs (*Uca*  
613 sp.), and to biogeochemical and hydrological processes associated with microtopography.

614 We further emphasize that pond formation *per se* is not directly driving permanent marsh loss, but it  
615 could lead to marsh loss in the pond runaway regime. In the pond runaway regime, an increase in the  
616 pond formation rate would directly increase the rate at which the marsh is lost, mainly by increasing the  
617 “seeds” from which ponds can expand. Pond formation is thus an example of a relatively secondary

618 mechanism that, through spatial interactions (Larsen, 2019), could lead to rapid marsh loss. Thus, we  
619 argue that future research should develop a mechanistic understanding of pond formation and determine  
620 whether environmental changes such climate or burrowing and grazing pressure, might increase the rate  
621 of pond formation.

## 622 **5.5 Marsh management**

623 All simulations were performed for scenarios in which the vegetated marsh keeps pace with RSLR. As  
624 such, if pond dynamics were not included, the marsh would have been preserved indefinitely and there  
625 would have not been any unvegetated area occupied by either ponds or mudflats. Thus, including pond  
626 dynamics in marshes where ponds are known to form is an essential step to simulate marsh evolution.

627 Including pond dynamics in marsh models is also essential for predicting ecosystem productivity. Marsh  
628 grasses remove CO<sub>2</sub> from the atmosphere and bury it in soils, support coastal food webs, and filter  
629 inorganic nutrients washed from the landscape, among other ecosystem services. As such, changes in  
630 productivity have consequences for ecological and biogeochemical processes within marshes and adjacent  
631 ecosystems. In both the mesotidal (Barnstable) and microtidal (Sage Lot Pond) simulations, normalized  
632 primary productivity increases monotonically with the RSLR rate (Fig. 9). The expansion of the  
633 unvegetated area for very high RSLR rates, however, starts to decrease productivity. For the microtidal  
634 case, a decrease in productivity associated with pond expansion could be observed even at the decadal  
635 time scale (Fig. 9B), and thus could be relevant for coastal management.

636 As previously identified (Mariotti, 2016), neither the presence of ponds nor the expansion of ponds is a  
637 sign of permanent marsh loss. On the other hand, the absence of pond recovery is a potential indicator of  
638 a regime shift. Monitoring pond recovery, such as by measuring their accretion rates once reconnected to  
639 the channel network, should thus become a routine marsh assessment, alongside measurements of vertical  
640 accretion in the vegetated marsh.

641 One management question is whether to promote or prevent pond recovery. One example includes  
642 selectively digging ditches to reconnect ponds, a strategy referred to as “quality ditching” or Open Water  
643 Marsh Management (Wolfe, 1996). Our model suggests that the appropriate management (in terms of  
644 morphological evolution of the salt marsh) depends on whether the marsh is in the pond recovery or pond  
645 runaway regime. In the former case, favoring pond drainage should accelerate vertical accretion, in the  
646 latter it would accelerate marsh loss.

647 As previously shown in a model that only considers one pond (Mariotti, 2016), determining whether a  
648 marsh is in the pond runaway or pond recovery regimes requires an estimate of the minimum inorganic  
649 deposition in the marsh interior ( $D_{cr}$ ), and specifically to estimate the suspended sediment concentration.  
650 Because this parameter is difficult to determine without long-term monitoring (Ganju et al., 2017), we  
651 suggest that analyzing the trajectory of recently connected ponds is important to determine whether ponds  
652 are recovering or expanding indefinitely.

## 653 **5.6 Model limitations and future directions**

654 The model assumes that any connected area above  $z_{min}$  revegetates instantaneously. Therefore, a mudflat  
655 is only present if  $z < z_{min}$ . In reality it could take several years for a connected pond to revegetate even if  
656  $z > z_{min}$ . For example, the recently connected ponds in Barnstable have not fully revegetated even if their  
657 elevation is  $\sim 1$  m above MSL (i.e.,  $z > z_{min}$ ). Even though this delay could be included in the dynamics, we  
658 argue that it is not crucial, because revegetation likely will occur within shorter times scales (decades)  
659 than the time scale considered in this study. More importantly, large vertical accretion rates by mud  
660 deposition could take place even though recently connected ponds are not fully revegetated.

661 Channels are assumed to be fixed. When analyzing historical imagery ( $\sim 50$  years), channels in Barnstable  
662 marsh are relatively stable, even though they could have migrated over longer time scales. Migrating  
663 channels would likely increase the rate at which ponds are intercepted and thus drained. Channel  
664 migration could be parameterized as a larger value for the reference drainage distance  $L$ , allowing ponds  
665 within the model to drain even if located at a large distance from channels. Indeed, this could be a

666 dominant mechanism for pond drainage at sites where channel migration is relatively fast (Finotello et al.,  
667 2018). Channel migration would likely result in similar marsh evolution dynamics and pond recovery,  
668 with marsh loss at the eroding bank but, at the same time, induce accretion that is faster than the RSRL  
669 rate at the accreting bank.

670 The model does not conserve sediment in the channel domain: the sediment transported from the bank to  
671 the channel through the creep mechanism does not accumulate in the channel, and the sediment  
672 transported from the channel to the marsh, which is responsible for the term  $D_m$ , does not cause a  
673 sediment deficit in the channel network. That is, we assume that there is an infinite supply of new  
674 sediment from the channels. In reality, a portion of the bank material that creeps into the channel would  
675 be resuspended and re-transported to the marsh platform, thus allowing for sediment recycling. This  
676 component cannot be reproduced in the model, since an explicit representation of the channel dynamics  
677 would be needed.

678 Finally, the model does not include the dynamics of hydrological alterations such as ditching, which is a  
679 common feature in New England salt marshes. Ditching could impact the marsh elevation dynamics in at  
680 least two ways. On one hand, ditches could cause a nearly instantaneous marsh-wide pond drainage,  
681 which could temporarily increase the spatially averaged vertical accretion rate. On the other hand, ditches  
682 could lower the water table and cause a combination of carbon oxidation and compaction, which in turn  
683 could lower the marsh elevation. Such effects could be included in the model by 1) allowing ponds close  
684 to the ditches to be drained similarly to the ponds drained by the natural channel network, and 2) adding  
685 an additional term in Eq. 1 to simulate a localized bed lowering close to the ditches.

## 686 **6. Conclusions**

687 The proposed model simulates the spatially explicit dynamics of marsh ponds, and thus allows simulation  
688 of the aggregated effect that ponds have on the evolution of the marsh platform. The Barnstable marsh is  
689 predicted to be in a pond recovery regime: pond expansion does not cause net marsh loss because they  
690 recover the marsh elevation once drained. Even in the pond recovery regime, however, ponds drastically

691 affect the marsh elevation and vertical accretion. In particular, pond dynamics explain why marsh vertical  
692 accretion, even away from channels, could be several times larger than the rate of RSLR, and also why  
693 the accretion rate is highly variable in space.

694 The model predicts that future increases in RSLR rate at Barnstable marsh would not cause the marsh to  
695 transition to the full pond runaway regime. Yet, with a large RSLR rate and a reduced sediment supply,  
696 ponds in the marsh interior might become permanent mudflats and thus increase the unvegetated area to  
697 ~20% of the total marsh. Monitoring of pond recovery, such as by measuring their accretion rates once  
698 reconnected to the channel network, could be used as a landscape-level indicator of regime shifts.

699 Marshes with a smaller tidal range and sediment supply, such as Sage Lot Pond marsh, are more prone to  
700 enter the pond runaway regime. For RSLR rates just above the critical threshold (e.g., 3 mm/yr), the rate  
701 of marsh loss by pond expansion is still relatively low, and the marsh could take several centuries (if not  
702 millennia) before completely disappearing. A further acceleration in RSLR rate (e.g., 5 mm/yr) would  
703 drastically increase the rate at which the marsh is lost by pond expansion – which will take place even  
704 though the vegetated marsh keeps pace with RSLR.

705 Future research needs include understanding the mechanism of pond formation, evaluating how  
706 hydrological alterations such as ditching affects pond dynamics, and quantifying how pond dynamics  
707 affect blue carbon accumulation and preservation.

708

## 709 **Acknowledgments**

710 We appreciate funding support for this work from Woods Hole Sea Grant (NA14OAR4170104 to ACS  
711 and GM) and NOAA NSC (NA14NOS4190145 to ACS, GM, MEG, and MT), USGS Coastal & Marine  
712 Geology Program, the USGS Land Change Science Program's LandCarbon program. We thank the  
713 Waquoit Bay National Estuarine Research Reserve and Sandy Neck Beach Park for providing research  
714 access. USGS staff including T. Wallace Brooks, Jennifer O'Keefe Suttles, Adrian Mann and Allyson

715 Boggess provided field and analytical support. Additional field support was provided by Claire Mayorga,  
716 Kelsey Gosselin, Madelyn Francesconi, and Sam MicNichol. Any use of trade, firm or product names is  
717 for descriptive purposes only and does not imply endorsement by the U.S. Government.

718

## 719 **References**

- 720 Adamowicz, S.C., Roman, C.T., 2005. New England salt marsh pools: A quantitative analysis of  
721 geomorphic and geographic features. *Wetlands* 25, 279–288. <https://doi.org/10.1672/4>
- 722 Appleby, P.G., Oldfield, F., 1978. The calculation of lead-210 dates assuming a constant rate of supply of  
723 unsupported <sup>210</sup>Pb to the sediment. *CATENA* 5, 1–8. [https://doi.org/10.1016/S0341-](https://doi.org/10.1016/S0341-8162(78)80002-2)  
724 [8162\(78\)80002-2](https://doi.org/10.1016/S0341-8162(78)80002-2)
- 725 Argow, B.A., FitzGerald, D.M., 2006. Winter processes on northern salt marshes: Evaluating the impact  
726 of in-situ peat compaction due to ice loading, Wells, ME. *Estuar. Coast. Shelf Sci., Salt Marsh*  
727 *Geomorphology: Physical and ecological effects on landform* 69, 360–369.  
728 <https://doi.org/10.1016/j.ecss.2006.05.006>
- 729 Argow, B.A., Hughes, Z.J., FitzGerald, D.M., 2011. Ice raft formation, sediment load, and theoretical  
730 potential for ice-rafted sediment influx on northern coastal wetlands. *Cont. Shelf Res.* 31, 1294–  
731 1305. <https://doi.org/10.1016/j.csr.2011.05.004>
- 732 Binford, M.W., 1990. Calculation and uncertainty analysis of <sup>210</sup>Pb dates for PIRLA project lake  
733 sediment cores. *J. Paleolimnol.* 3, 253–267. <https://doi.org/10.1007/BF00219461>
- 734 Brush, T., Lent, R.A., Hruby, T., Harrington, B.A., Marshall, R.M., Montgomery, W.G., 1986. Habitat  
735 Use by Salt Marsh Birds and Response to Open Marsh Water Management. *Colon. Waterbirds* 9,  
736 189–195. <https://doi.org/10.2307/1521212>
- 737 Cavatorta, J.R., Johnston, M., Hopkinson, C., Valentine, V., 2003. Patterns of sedimentation in a salt  
738 marsh-dominated estuary. *Biol. Bull.* 205, 239–241.
- 739 Christiansen, T., Wiberg, P.L., Milligan, T.G., 2000. Flow and Sediment Transport on a Tidal Salt Marsh  
740 Surface. *Estuar. Coast. Shelf Sci.* 50, 315–331. <https://doi.org/10.1006/ecss.2000.0548>
- 741 Cutshall, N.H., Larsen, I.L., Olsen, C.R., 1983. Direct analysis of <sup>210</sup>Pb in sediment samples: Self-  
742 absorption corrections. *Nucl. Instrum. Methods Phys. Res.* 206, 309–312.  
743 [https://doi.org/10.1016/0167-5087\(83\)91273-5](https://doi.org/10.1016/0167-5087(83)91273-5)
- 744 Elsey-Quirk, T., Mariotti, G., Valentine, K., Raper, K., 2019. Retreating marsh shoreline creates hotspots  
745 of high-marsh plant diversity. *Sci. Rep.* 9, 5795. <https://doi.org/10.1038/s41598-019-42119-8>
- 746 Fagherazzi, S., Kirwan, M.L., Mudd, S.M., Guntenspergen, G.R., Temmerman, S., D’Alpaos, A., Koppel,  
747 J., Rybczyk, J.M., Reyes, E., Craft, C., others, 2012. Numerical models of salt marsh evolution:  
748 Ecological, geomorphic, and climatic factors. *Rev. Geophys.* 50.
- 749 Finotello, A., Lanzoni, S., Ghinassi, M., Marani, M., Rinaldo, A., D’Alpaos, A., 2018. Field migration  
750 rates of tidal meanders recapitulate fluvial morphodynamics. *Proc. Natl. Acad. Sci.* 115, 1463–  
751 1468. <https://doi.org/10.1073/pnas.1711330115>
- 752 Ganju, N.K., Defne, Z., Kirwan, M.L., Fagherazzi, S., D’Alpaos, A., Carniello, L., 2017. Spatially  
753 integrative metrics reveal hidden vulnerability of microtidal salt marshes. *Nat. Commun.* 8.  
754 <https://doi.org/10.1038/ncomms14156>
- 755 Gonnee, M.E., Maio, C.V., Kroeger, K.D., Hawkes, A.D., Mora, J., Sullivan, R., Madsen, S., Buzard,  
756 R.M., Cahill, N., Donnelly, J.P., 2019. Salt marsh ecosystem restructuring enhances elevation  
757 resilience and carbon storage during accelerating relative sea-level rise. *Estuar. Coast. Shelf Sci.*  
758 217, 56–68. <https://doi.org/10.1016/j.ecss.2018.11.003>

759 Gonneea, M.E., O’Keefe Suttles, J.A., Kroeger, K.D., 2018. Collection, analysis, and age-dating of  
760 sediment cores from salt marshes on the south shore of Cape Cod, Massachusetts, from 2013  
761 through 2014. US Geol. Surv. Data Release <https://doi.org/10.5066/F7H41QPP>.

762 Harshberger, J.W., 1909. The Vegetation of the Salt Marshes and of the Salt and Fresh Water Ponds of  
763 Northern Coastal New Jersey. *Proc. Acad. Nat. Sci. Phila.* 61, 373–400.

764 Hopkinson, C.S., Morris, J.T., Fagherazzi, S., Wollheim, W.M., Raymond, P.A., 2018. Lateral Marsh  
765 Edge Erosion as a Source of Sediments for Vertical Marsh Accretion. *J. Geophys. Res.*  
766 *Biogeosciences* 123, 2444–2465. <https://doi.org/10.1029/2017JG004358>

767 Howes, N.C., FitzGerald, D.M., Hughes, Z.J., Georgiou, I.Y., Kulp, M.A., Miner, M.D., Smith, J.M.,  
768 Barras, J.A., 2010. Hurricane-induced failure of low salinity wetlands. *Proc. Natl. Acad. Sci.* 107,  
769 14014–14019. <https://doi.org/10.1073/pnas.0914582107>

770 Johnston, M.E., Cavatorta, J.R., Hopkinson, C.S., Valentine, V., 2003. Importance of metabolism in the  
771 development of salt marsh ponds. *Biol. Bull.* 205, 248–249.

772 Kesel, R.H., Smith, J.S., 1978. Tidal creek and pan formation in intertidal salt marshes, Nigg Bay,  
773 Scotland. *Scott. Geogr. Mag.* 94, 159–168. <https://doi.org/10.1080/00369227808736403>

774 Kirwan, M., Temmerman, S., 2009. Coastal marsh response to historical and future sea-level acceleration.  
775 *Quat. Sci. Rev., Quaternary Ice Sheet-Ocean Interactions and Landscape Responses* 28, 1801–  
776 1808. <https://doi.org/10.1016/j.quascirev.2009.02.022>

777 Kirwan, M.L., Murray, A.B., 2008. Tidal marshes as disequilibrium landscapes? Lags between  
778 morphology and Holocene sea level change. *Geophys. Res. Lett.* 35, L24401.  
779 <https://doi.org/10.1029/2008GL036050>

780 Kirwan, M.L., Murray, A.B., 2007. A coupled geomorphic and ecological model of tidal marsh evolution.  
781 *Proc. Natl. Acad. Sci.* 104, 6118–6122. <https://doi.org/10.1073/pnas.0700958104>

782 Kirwan, M.L., Murray, A.B., Boyd, W.S., 2008. Temporary vegetation disturbance as an explanation for  
783 permanent loss of tidal wetlands. *Geophys. Res. Lett.* 35, n/a–n/a.  
784 <https://doi.org/10.1029/2007GL032681>

785 Koop-Jakobsen, K., Gutbrod, M.S., 2019. Shallow Salt Marsh Tidal Ponds—An Environment With  
786 Extreme Oxygen Dynamics. *Front. Environ. Sci.* 7. <https://doi.org/10.3389/fenvs.2019.00137>

787 Larsen, L.G., 2019. Multiscale flow-vegetation-sediment feedbacks in low-gradient landscapes.  
788 *Geomorphology* 334, 165–193. <https://doi.org/10.1016/j.geomorph.2019.03.009>

789 Leonardi, N., Ganju, N.K., Fagherazzi, S., 2016. A linear relationship between wave power and erosion  
790 determines salt-marsh resilience to violent storms and hurricanes. *Proc. Natl. Acad. Sci.* 113, 64–  
791 68.

792 Marani, M., Belluco, E., D’Alpaos, A., Defina, A., Lanzoni, S., Rinaldo, A., 2003. On the drainage  
793 density of tidal networks. *Water Resour. Res.* 39, 1040. <https://doi.org/10.1029/2001WR001051>

794 Marani, M., D’Alpaos, A., Lanzoni, S., Santalucia, M., 2011. Understanding and predicting wave erosion  
795 of marsh edges. *Geophys. Res. Lett.* 38, L21401. <https://doi.org/10.1029/2011GL048995>

796 Marani, M., Lio, C.D., D’Alpaos, A., 2013. Vegetation engineers marsh morphology through multiple  
797 competing stable states. *Proc. Natl. Acad. Sci.* 201218327.  
798 <https://doi.org/10.1073/pnas.1218327110>

799 Mariotti, G., 2018. Marsh channel morphological response to sea level rise and sediment supply. *Estuar.*  
800 *Coast. Shelf Sci.* <https://doi.org/10.1016/j.ecss.2018.05.016>

801 Mariotti, G., 2016. Revisiting salt marsh resilience to sea level rise: Are ponds responsible for permanent  
802 land loss? *J. Geophys. Res. Earth Surf.* 121, 1391–1407. <https://doi.org/10.1002/2016JF003900>

803 Mariotti, G., Canestrelli, A., 2017. Long-term morphodynamics of muddy backbarrier basins: Fill in or  
804 empty out? *Water Resour. Res.* 53, 7029–7054. <https://doi.org/10.1002/2017WR020461>

805 Mariotti, G., Kearney, W., Fagherazzi, S., 2016. Soil creep in salt marshes. *Geology* 44, 459–462.

806 Mariotti, G., Kearney, W.S., Fagherazzi, S., 2019. Soil creep in a mesotidal salt marsh channel bank: Fast,  
807 seasonal, and water table mediated. *Geomorphology* 334, 126–137.  
808 <https://doi.org/10.1016/j.geomorph.2019.03.001>



809 McKee, K.L., Patrick, W.H., Jr., 1988. The relationship of smooth cordgrass (*Spartina Alterniflora*) to  
810 tidal datums: A review. *Estuaries* 11, 143–151. <https://doi.org/10.2307/1351966>

811 Morris, J.T., Barber, D.C., Callaway, J.C., Chambers, R., Hagen, S.C., Hopkinson, C.S., Johnson, B.J.,  
812 Megonigal, P., Neubauer, S.C., Troxler, T., Wigand, C., 2016. Contributions of organic and  
813 inorganic matter to sediment volume and accretion in tidal wetlands at steady state. *Earths Future*  
814 4, 110–121. <https://doi.org/10.1002/2015EF000334>

815 Morris, J.T., Sundareshwar, P.V., Nietch, C.T., Kjerfve, B., Cahoon, D.R., 2002. Responses of coastal  
816 wetlands to rising sea level. *Ecology* 83, 2869–2877. <https://doi.org/10.2307/3072022>

817 Nyman, J.A., Carloss, M., Delaune, R.D., Patrick, W.H., 1994. Erosion rather than plant dieback as the  
818 mechanism of marsh loss in an estuarine marsh. *Earth Surf. Process. Landf.* 19, 69–84.  
819 <https://doi.org/10.1002/esp.3290190106>

820 OCM Partners, 2019. 2013–2014 U.S. Geological Survey CMGP LiDAR: Post Sandy (MA, NH,  
821 RI), <https://inport.nmfs.noaa.gov/inport/item/49846>.

822 Pethick, J.S., 1974. The distribution of salt pans on tidal salt marshes. *J. Biogeogr.* 1, 57–62.  
823 <https://doi.org/10.2307/3038068>

824 Redfield, A.C., 1972. Development of a New England Salt Marsh. *Ecol. Monogr.* 42, 201–237.  
825 <https://doi.org/10.2307/1942263>

826 Redfield, A.C., 1965. Ontogeny of a Salt Marsh Estuary. *Science* 147, 50–55.  
827 <https://doi.org/10.1126/science.147.3653.50>

828 Schepers, L., Kirwan, M., Guntenspergen, G., Temmerman, S., 2017. Spatio-temporal development of  
829 vegetation die-off in a submerging coastal marsh. *Limnol. Oceanogr.* 62, 137–150.  
830 <https://doi.org/10.1002/lno.10381>

831 Spivak, A.C., Gosselin, K., Howard, E., Mariotti, G., Forbrich, I., Stanley, R., Sylva, S.P., 2017. Shallow  
832 ponds are heterogeneous habitats within a temperate salt marsh ecosystem. *J. Geophys. Res.*  
833 *Biogeosciences* 122, 1371–1384. <https://doi.org/10.1002/2017JG003780>

834 Spivak, A.C., Gosselin, K.M., Sylva, S.P., 2018. Shallow ponds are biogeochemically distinct habitats in  
835 salt marsh ecosystems. *Limnol. Oceanogr.* 63, 1622–1642. <https://doi.org/10.1002/lno.10797>

836 van Huissteden, J., van de Plassche, O., 1998. Sulphate reduction as a geomorphological agent in tidal  
837 marshes ('Great Marshes' at Barnstable, Cape Cod, USA). *Earth Surf. Process. Landf.* 23, 223–  
838 236. [https://doi.org/10.1002/\(SICI\)1096-9837\(199803\)23:3<223::AID-ESP843>3.0.CO;2-I](https://doi.org/10.1002/(SICI)1096-9837(199803)23:3<223::AID-ESP843>3.0.CO;2-I)

839 Wasson, K., Ganju, N.K., Defne, Z., Endris, C., Elsey-Quirk, T., Thorne, K.M., Freeman, C.M.,  
840 Guntenspergen, G., Nowacki, D.J., Raposa, K.B., 2019. Understanding tidal marsh trajectories:  
841 evaluation of multiple indicators of marsh persistence. *Environ. Res. Lett.* 14, 124073.  
842 <https://doi.org/10.1088/1748-9326/ab5a94>

843 Wilson, C.A., Hughes, Z.J., FitzGerald, D.M., Hopkinson, C., Valentine, V., Kolker, A.S., 2014.  
844 Saltmarsh Pool and Tidal Creek Morphodynamics: Dynamic Equilibrium of Northern Latitude  
845 Saltmarshes? *Geomorphology*. <https://doi.org/10.1016/j.geomorph.2014.01.002>

846 Wilson, K.R., Kelley, J.T., Croitoru, A., Dionne, M., Belknap, D.F., Steneck, R., 2009. Stratigraphic and  
847 Ecophysical Characterizations of Salt Pools: Dynamic Landforms of the Webhannet Salt Marsh,  
848 Wells, ME, USA. *Estuaries Coasts* 32, 855–870. <https://doi.org/10.1007/s12237-009-9203-7>

849 Wilson, K.R., Kelley, J.T., Tanner, B.R., Belknap, D.F., 2010. Probing the origins and stratigraphic  
850 signature of salt pools from north-temperate marshes in Maine, U.S.A. *J. Coast. Res.* 1007–1026.  
851 <https://doi.org/10.2112/JCOASTRES-D-10-00007.1>

852 Wolfe, R.J., 1996. Effects of open marsh water management on selected tidal marsh resources: a review.  
853 *J. Am. Mosq. Control Assoc.* 12, 701–712.

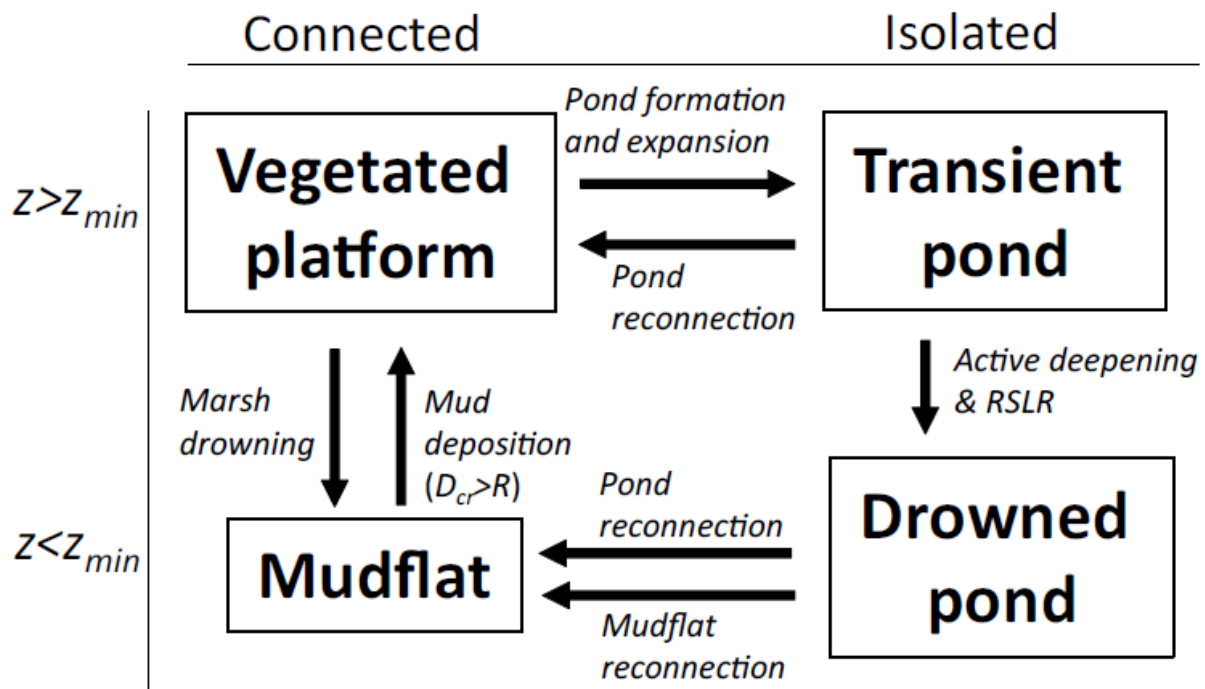
854

855 **List of figures**

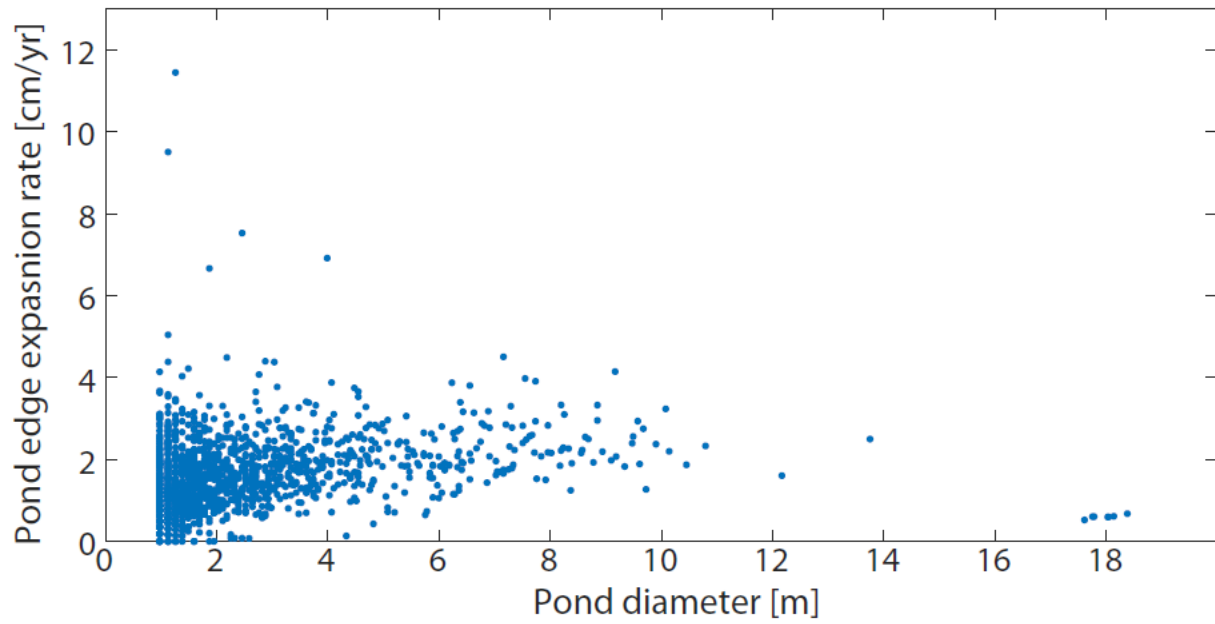


856

857 Figure 1. A) Map of the study area including Barnstable marsh and Sage Lot Pond marsh (Massachusetts,  
 858 USA). B) Sage Lot Pond marsh, C) Barnstable marsh. The dashed rectangle outlines the domain used in  
 859 the model. The white dots indicate the locations where SSC was measured in triplicates. The red dots  
 860 indicated the location where cores for vertical accretion were collected. D,E,F) Example of pond  
 861 reconnection and rapid revegetation (the pond is indicated by the arrow on the bottom right of panel C).  
 862 G) Location of the surveyed ponds. Red dots indicate ponds surveyed along a transect (showed in Fig. 8),  
 863 white dots indicate ponds only surveyed at one edge. H) Detail of a marsh core collected adjacent to the  
 864 channel. Images from Google Earth (NASA, USDA) accessed on October 2019.



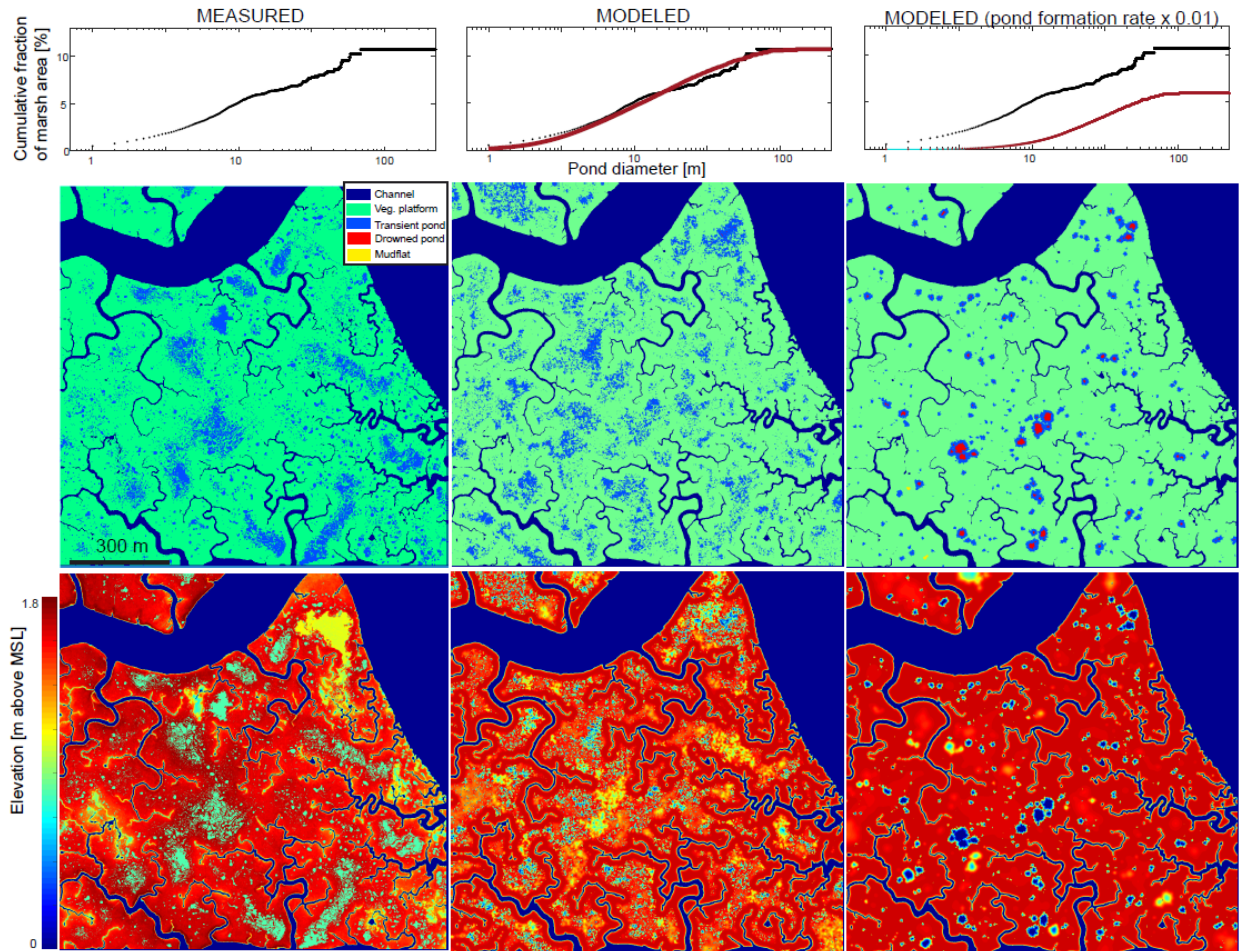
865  
 866 Figure 2. Summary schematic of the marsh and pond dynamics and scheme of the various sediment fluxes  
 867 in the model. Net vertical accretion is equal to the gross vertical deposition minus bank creep and  
 868 ponding.



869

870 Figure 3. Measured pond edge expansion rate as the increase of the pond radius through time in

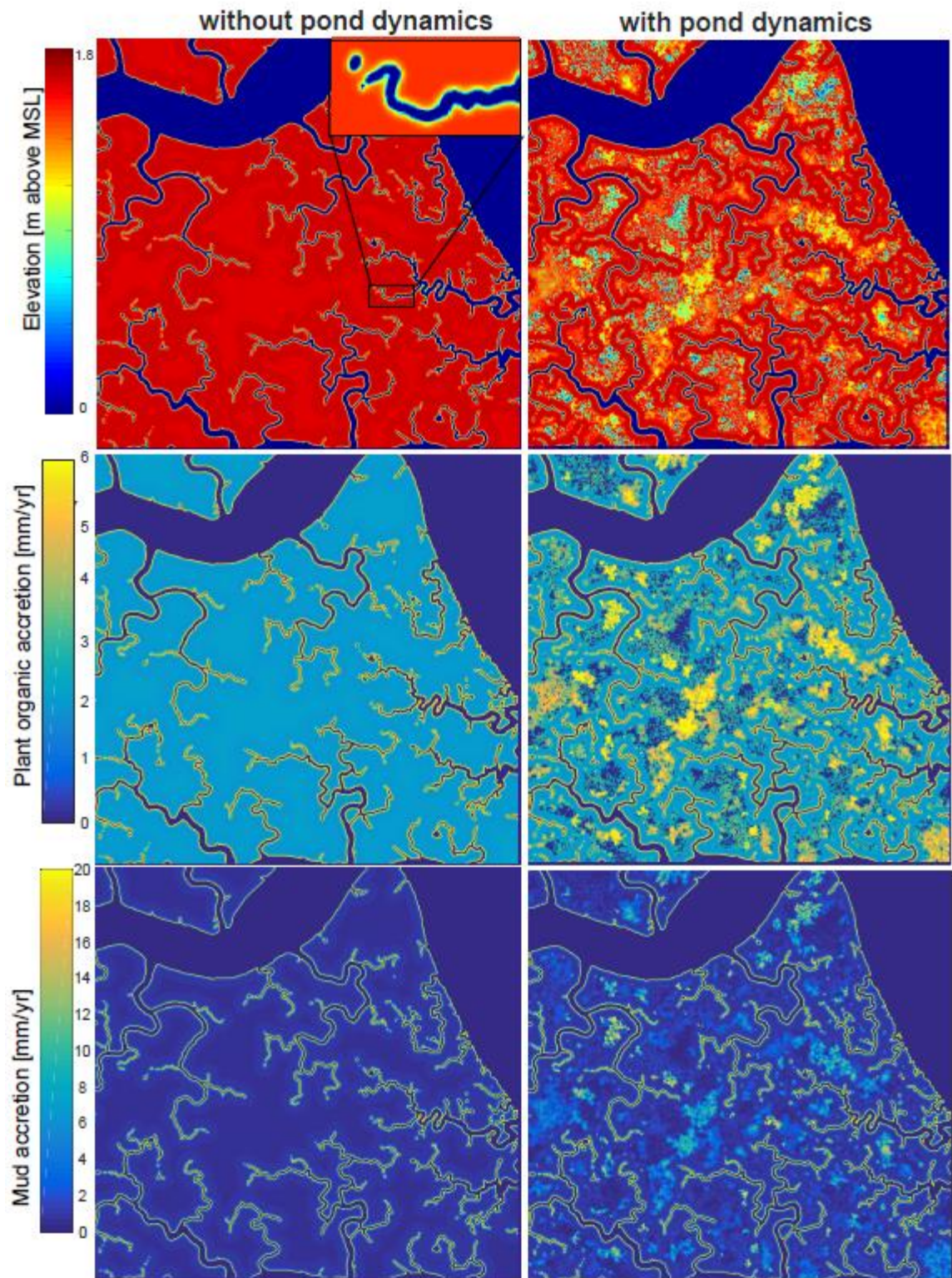
871 Barnstable marsh from 1973 to 2014 as a function of the pond diameter.



872

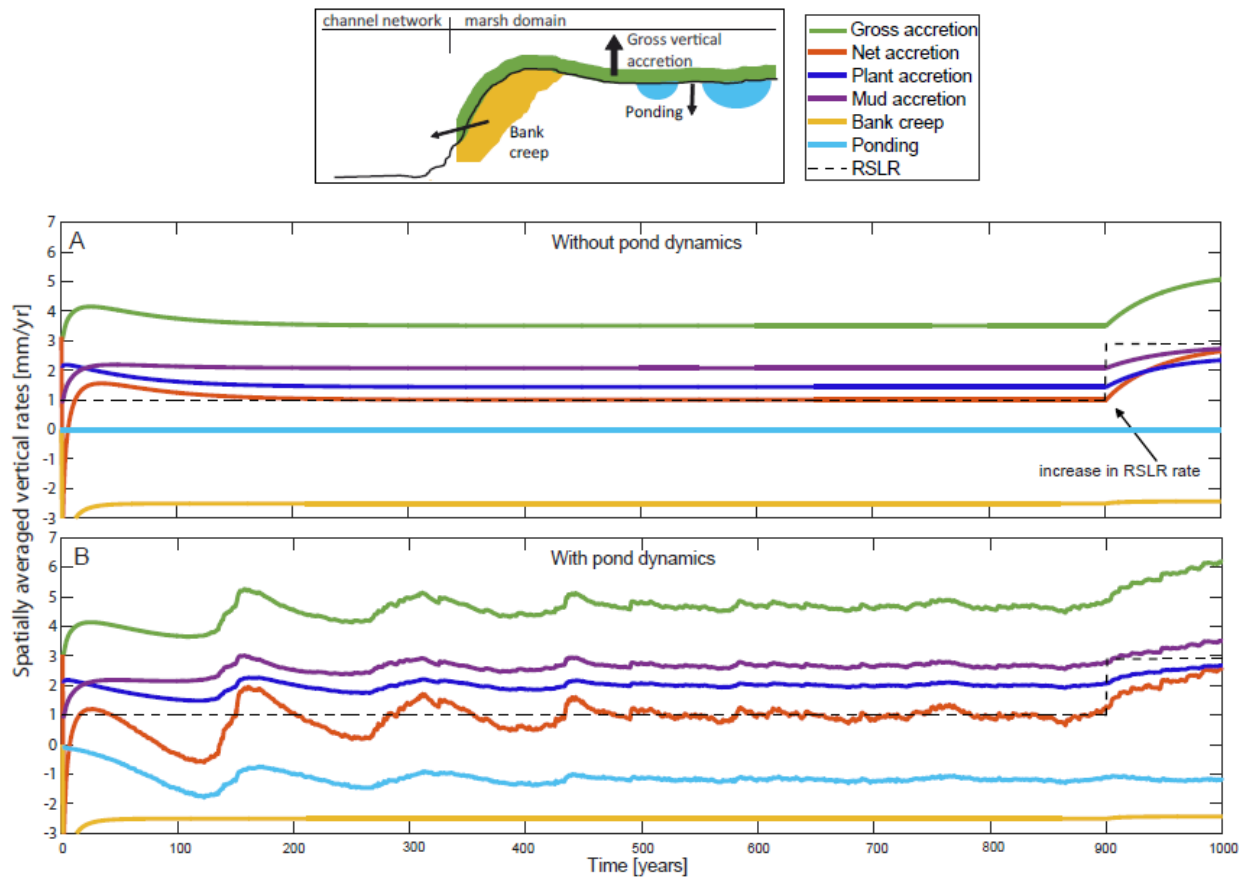
873 Figure 4. A,B,C) Comparison of measured and simulated (at steady state after 1000 years) pond size  
 874 distribution. A) Measured pond size distribution, showing that the total fraction of pond area is about 10%  
 875 of the marsh surface. B) Best fit for the parameters  $k_{seed}$  and  $k_{exp}$ . C) Model results for the case in which  
 876  $k_{seed}$  is decreased by a factor 100. D,G) Measured pond spatial distribution and elevation E,F,H,I) Model  
 877 snapshot after 1000 years showing the pond spatial distribution and the elevation (as the last datapoint in  
 878 Fig. 6).

879



881 Figure 5. Vertical accretion rate by *in situ* plant production and by mud accumulation for the case with  
 882 and without pond dynamics calculated at year 1000 (as the last datapoint in Fig. 6). The inset in the top  
 883 left panels shows the detail of the low-marsh adjacent to a channel.

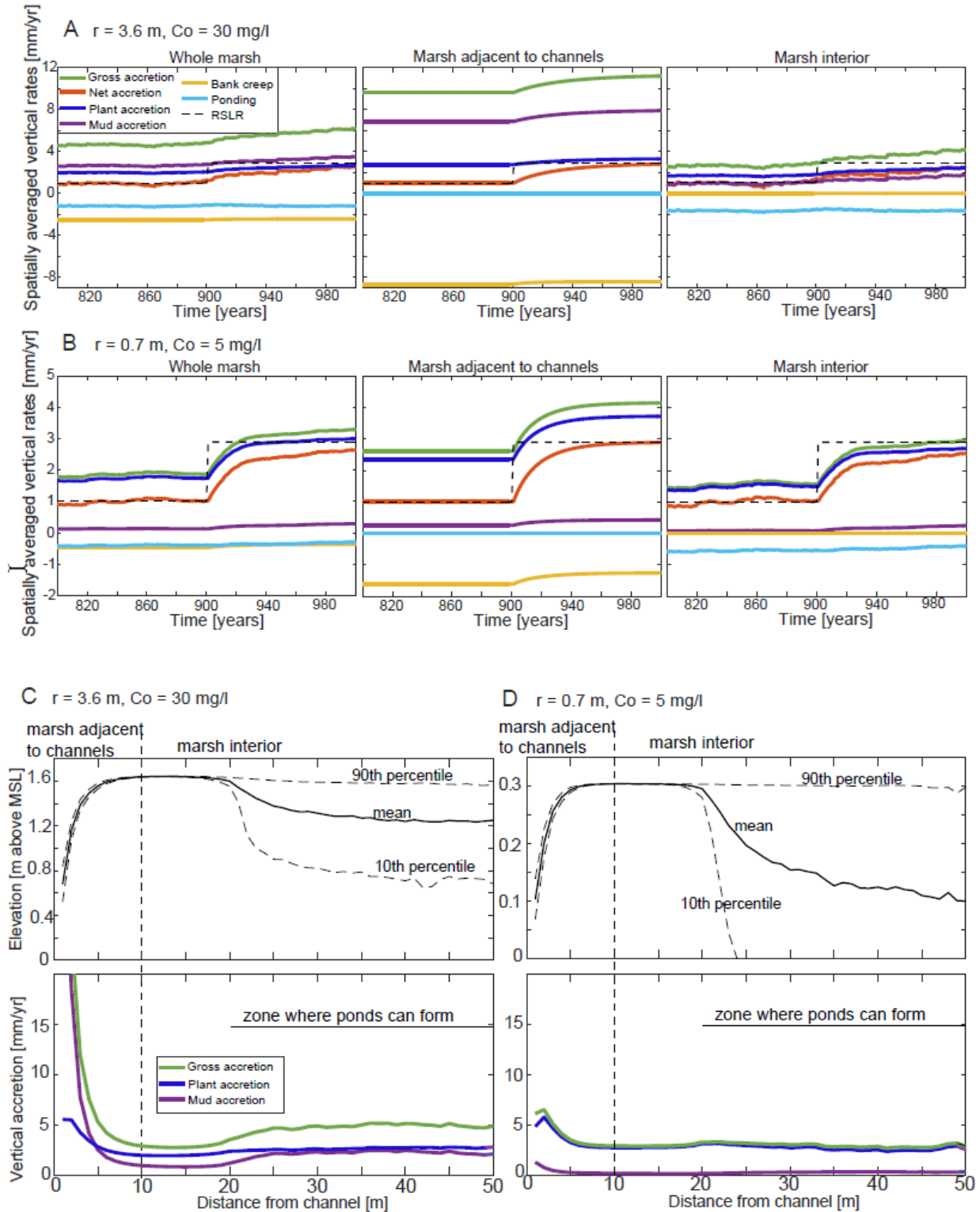
884



885

886 Figure 6. Reconstructed time series of spatially-averaged elevation change for Barnstable marsh,  
 887 comparing the case without ponds dynamics (A) and with pond dynamics (B). Gross accretion is the sum  
 888 of plant and mud accretion. Net accretion is the gross accretion minus ponding and bank creep. Note that  
 889 during the first ~500 years the marsh is equilibrating from the initial conditions without ponds.

890

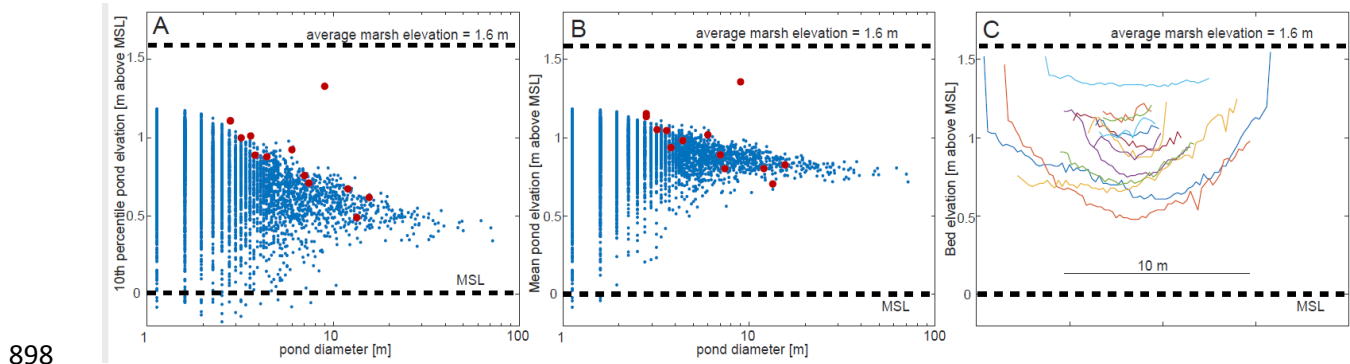


891

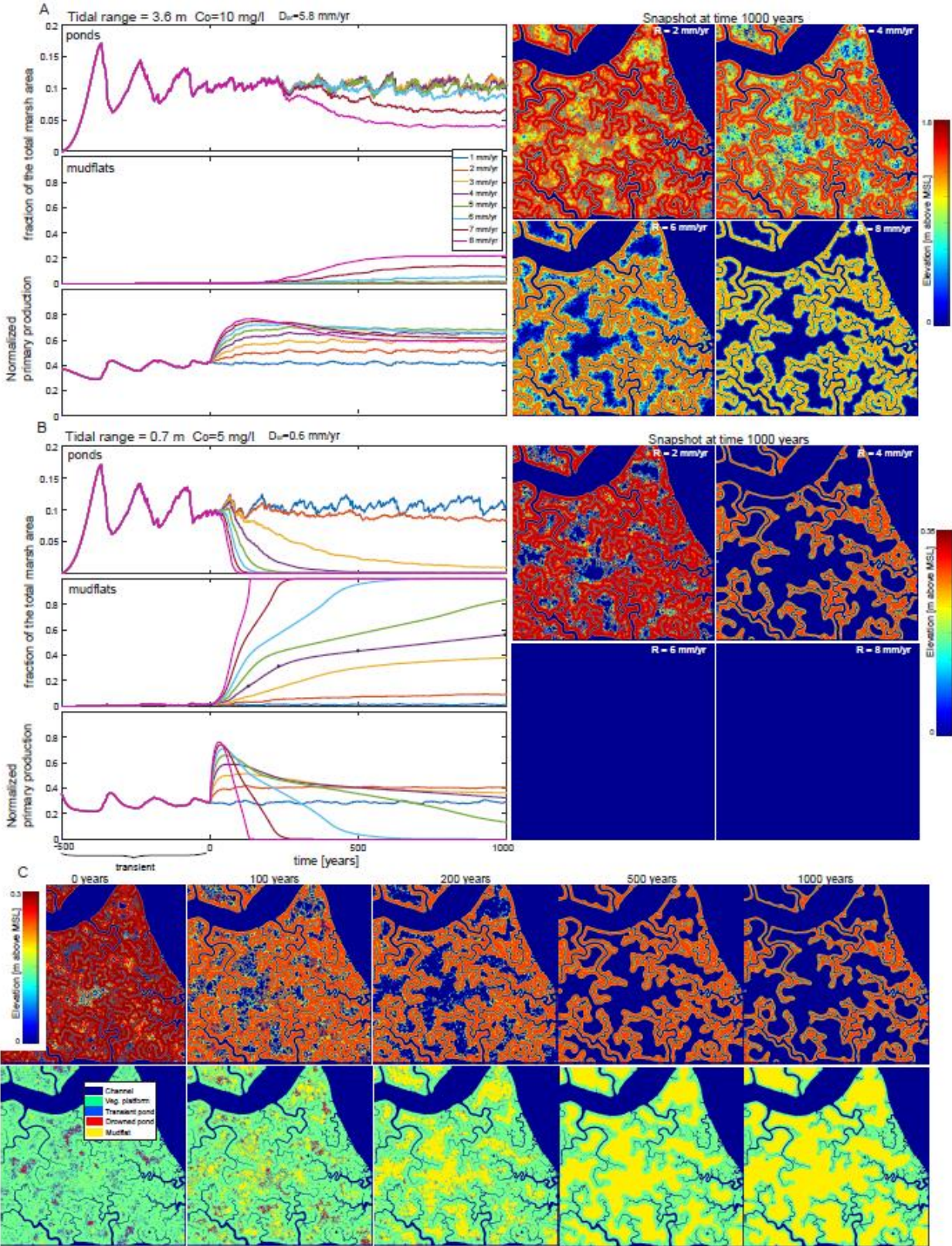
892 Figure 7. A,B) Spatially-averaged elevation change during the transition from  $R=1 \text{ mm/yr}$  to  $R=2.9$   
 893  $\text{mm/yr}$  (as in Fig. 6B), considering the whole marsh area, the area adjacent to channels, and the marsh



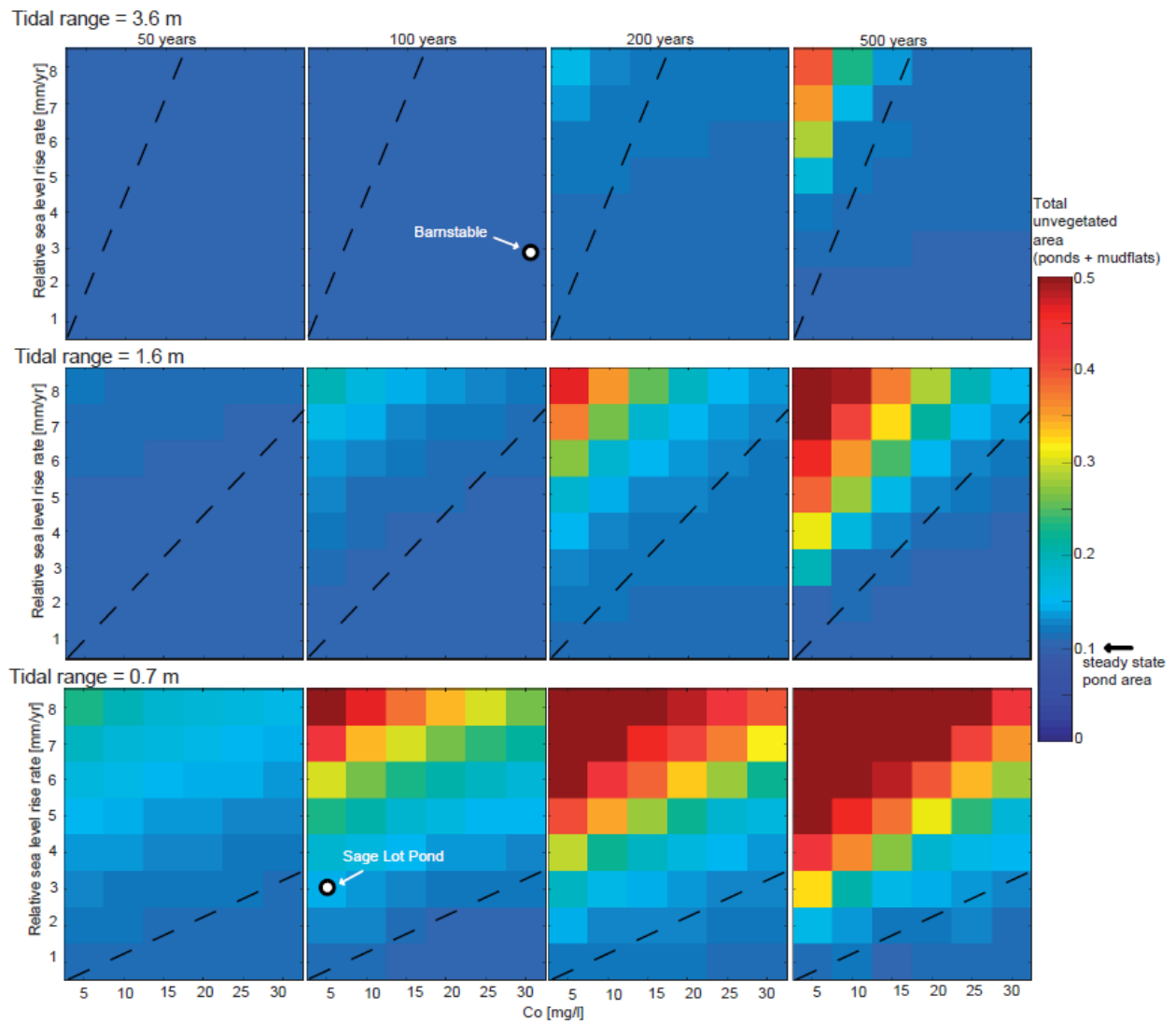
894 interior. Note that in the marsh interior the bank creep is zero. C,D) Snapshot at year 1000 showing the  
 895 how the vertical accretion varies rapidly with the distance from the channel network. A,C) Conditions  
 896 representing Barnstable marsh ( $r=3.6$  m,  $C_o=30$  mg/l), B,D) Conditions representing Sage Lot Pond  
 897 marsh ( $r=0.7$  m,  $C_o=5$  mg/l).



899 Figure 8. A,B) Modeled 10<sup>th</sup> percentile (A) and mean (B) pond elevation as a function of pond size. The  
 900 blue dots are the individual points from the model, the red dots are the survey of the 13 ponds in  
 901 Barnstable marsh. C) Cross sections of the 13 ponds surveyed in Barnstable marsh (see Fig 1G).



903 Figure 9. A,B) Amount of pond and mudflat area through time for different RSLR rates for the case of  
 904 Barnstable marsh ( $r=3.6$  m) with a reduced sediment supply ( $C_o=10$  mg/l) (A), and for the case of Sage  
 905 Lot Pond marsh ( $r=0.7$  m and  $C_o=5$  mg/l) (B). The normalized primary production is calculated averaging  
 906 the plant primary production divided by the maximum primary production (which is attained when the  
 907 marsh is at the elevation optimum). The normalized primary production initially increases because the  
 908 marsh attains a lower elevation but subsequently decreases when the pond area (whose primary  
 909 production is assumed to be zero) increases. C) Snapshots of marsh configurations at different times (as  
 910 indicated by the black dots in panel B) for the case of Sage Lot Pond marsh with  $R=4$  mm/yr.



911

912 Figure 10. Predictions of total unvegetated area (ponds + mudflats) at different time intervals after the  
 913 increase in RSLR rate. The dashed lines indicate the threshold between pond recovery and pond runaway  
 914 regime using the lumped pond model of Mariotti (2018), with  $R=D_{cr}=\alpha C_o r/(2T\rho_m)$ . The comparison with  
 915 Barnstable and Sage Lot Pond marsh is made assuming that the increase in relative sea level rise rate  
 916 started about 100 years ago at the beginning of the 20<sup>th</sup> century.

917

918 Table 1. Sediment accretion rates measured on 1 cm sediment core intervals in Barnstable (measured  
 919 for this work) and Sage Lot Pond marshes (Gonneea et al., 2019, 2018).

920

Site	Sediment accretion rate (1900 to 2018) mm/y
<b>Sage Lot Pond</b>	
Interior (1 core, 13 intervals)	1.4 ± 0.3
Channel-adjacent (1 core, 27 intervals)	3.6 ± 2.0
<b>Barnstable</b>	
Interior (3 cores, 134 intervals)	5.1 ± 3.3
Channel-adjacent (3 cores, 130 intervals)	4.6 ± 2.5

921

922 Table 2. List of parameters used in the model.

	Symbol	Description	Value	Reference
	$\Delta x$	Spatial discretization	1 m	
	$\Delta t$	Temporal discretization	1 year	
Physical parameters	$C_o$	SSC in channels	30 mg/l or 5 mg/l	Measured
	$\rho_m$	Mud dry bulk density	650 kg/m <sup>3</sup>	Assumed
	$\beta$	Horizontal decay rate of SSC with distance from channel network	0.05 m <sup>-1</sup>	(Christiansen et al., 2000)
	$\alpha$	Fraction of spatially uniform SSC	0.3	Assumed

	$r$	Spring tidal range	3.6 m or 0.7 m	NOAA Station 8447930 and Station 8447241
	$\Delta r$	Spring-neap variability	$0.05r$	NOAA
	$T$	Tidal period	12.5 hr	NOAA
	$R$	Relative Sea Level Rise rate	2.9 mm/yr	NOAA
	$\mu$	Soil creep diffusivity	$0.1 \text{ m}^2/\text{yr}$	(Mariotti et al., 2019)
Vegetation parameters	$z_{min}$	Min elevation for vegetation	0	Assumed
	$z_{max}$	Max elevation for vegetation	$r/2$	Assumed
	$D_{pMAX}$	Max in-situ organic deposition	6 mm/yr	Assumed
Pond Parameters	$k_{seed}$	Pond formation rate	$4 \cdot 10^{-4}$ #ponds/m <sup>2</sup> /yr	Calibrated
	$k_{exp}$	Pond expansion rate	0.015 m/yr	Measured
	$L$	Drainage influence length	20 m	Measured
	$Y_{pond}$	Max initial depth of new ponds	$0.25(z_{max} - z_{min})$	Calibrated
	$P_{deepening}$	Active deepening of ponds	3 mm/yr	Calibrated

923

924